cytochalasin D or 0–5 mM amiloride (all from Sigma-Aldrich, St Louis, MO, USA). After the PTD-FAMs were added, cells were maintained for 1 h (30 min for amiloride) in the presence of inhibitors and washed several times with phosphate-buffered saline. As a control, the cellular uptake of transferrin fluorescein isothiocyanate (Invitrogen) was also monitored.

Cell proliferation assay

Cell viability was determined using a WST-8 assay kit (Nacalai Tesque, Kyoto, Japan) according to the manufacturer's instructions. The assay is based on the cleavage of the tetrazolium salt WST-8 to formazan by cellular mitochondrial dehydrogenase. HeLa cells were cultured in 96-well plates (Nalge Nunc International) at 5.0×10^3 cells per well in MEMα and incubated for 24 h at 37 °C. Jurkat cells were cultured in 96-well plates at 1.0×10^4 cells per well in Dulbecco's modified Eagle's medium. The cells were treated with various concentrations of PTD-biotin. After 24 h incubation, cell viability was measured using the WST-8 assay kit.

Membrane integrity assay

The lactate dehydrogenase (LDH) leakage assay was used to quantify the membrane integrity of the PTD-treated cells. This assay detects the amount of LDH released into the culture media as a result of plasma membrane disruption after PTD treatment. HeLa cells were cultured in 96-well plates (Nalge Nunc International) at 5.0×10^3 cells per well in MEMα and incubated for 24 h at 37 °C. Jurkat cells were cultured in 96-well plates at 1.0×10^4 cells per well in Dulbecco's modified Eagle's medium. Each cell type was treated with various concentrations of PTD-biotin. After 3 h incubation, the LDH release activity of the peptides was measured using an LDH cytotoxicity test (Wako) according to the manufacturer's instructions.

Expression and purification of PTD-fused Venus protein

The Venus (variant of yellow fluorescent protein) DNA sequence was kindly provided by Dr A Miyawaki (RIKEN Brain Science Institute). The Tat-Venus DNA sequence was amplified by PCR. At the 5′ end, the primer sequence 5′-TTTAAGAAGGAGATATACATATGGCTTACGGTCGTAAAAAA CGTCGCCAGCGTCGCCGTGGTGGCGGCGGTTCCCTCGA GCACCACCATCACCACCATGTGAGCAAGGGCGAGGAGC TGTTCAC-3′ introduced an *Nde* I site and Tat sequence and at the 3′ end, the primer sequence 5′-GCTTTGTTAGCAG CCGAATTCTTACTTGTACAGCTCGTCCATGCCGAGAGTGA TC-3′ introduced an *Eco* RI site. The PCR product was digested with *Nde* I and *Eco* RI and inserted into a protein expression plasmid. Other plasmids expressing Antp-, Rev- or VP22-Venus recombinant proteins were constructed by replacing the Tat-coding region in the Tat-Venus plasmid with the Antp, Rev or VP22 sequences using the *Nde* I and *Xho* I restriction sites. These sequences were obtained by annealing the following oligonucleotides with protruding single-strand DNA corresponding to the *Nde* I and *Xho* I sites: Antp sense, 5′-TATGGCTCGTCAGATCAAAATCTGGTTCCA GAATCGTCGTATGAAGTGGAAAAAAGGTGGCGGCGGTTC CC-3′; Antp antisense, 5′-TCGAGGGAACCGCCGCCACCTT TTTTCCACTTCATACGACGATTCTGGAACCAGATTTTGATC TGACGAGCCA-3′; Rev sense, 5′-TATGGCTACCCGTCAGGC TCGTCGTAATCGTCGTCGTCGTTGGCGTGAACGTCAGCGT GGTGGCGGCGGTTCCC-3′; Rev antisense, 5′-TCGAGGGAA CCGCCGCCACCACGCTGACGTTCACGCCAACGACGACGA CGATTACGACGAGCCTGACGGGTAGCCA-3′; VP22 sense, 5′-TATGGCTAACGCTAAAACCCGTCGTCACGAACGTCGTCG TAAACTGGCTATCGAACGTGGTGGCGGCGGTTCCC-3′; VP22 antisense, 5′-TCGAGGGAACCGCCGCCACCACGTTCGATAG CCAGTTTACGACGACGTTCGTGACGACGGGTTTTAGCGT TAGCCA-3′. The plasmids, except for the Antp-Venus expression vector, were transformed into *Escherichia coli* BL21 Star (DE3) (Invitrogen). The Antp-Venus-expressing vector was transformed into BL21 Star (DE3), in which the plasmid-expressing chaperone (pGro7) was pretransformed. Transformed *E. coli* was cultured and the cell paste was suspended in BugBuster Master Mix (Novagen, Darmstadt, Germany) and centrifuged. PTD-Venus was recovered in the supernatant and purified by His-tag affinity purification and gel filtration chromatography.

Confocal laser scanning microscopy analysis

HeLa cells were cultured on Lab-Tek II Chambered Coverglass (Nalge Nunc International) at 3.0×10^4 cells per well in MEMα supplemented with 10% FBS and incubated for 24 h at 37 °C. Internalization of PTD-FAM or PTD-Venus was performed as follows: HeLa cells were treated with PTD-FAM or PTD-Venus (10 μM) in Opti-MEM I containing 100 ng ml^{-1} Hoechst 33342 (Invitrogen) and 6 μg ml^{-1} FM4-64 (Invitrogen). After incubation at 37 °C for 3 h, the medium was exchanged with fresh medium and fluorescence was observed by confocal laser scanning microscopy (Leica Microsystems GmbH, Wetzlar, Germany) without cell fixation. For cotreatment with HA2-Tat, HeLa cells were cotreated with PTD-FAM (10 μM) and HA2-Tat (2 μM) in Opti MEM I containing 100 ng ml^{-1} Hoechst 33342. After incubation at 37 °C for 3 h, the medium was exchanged with fresh medium and fluorescence was observed by confocal laser scanning microscopy without cell fixation.

Results

Comparison of transduction efficiency and cytotoxicity of four PTDs

To confirm the intracellular translocation activity of the four selected PTDs, we evaluated the transduction efficiency of Tat-, Antp-, Rev- and VP22-FAM in six cell lines (adherent: HeLa, HaCaT and A431 cells; nonadherent: Jurkat, MOLT-4 and HL60 cells) using flow cytometric analysis (Figure 1). These PTDs contain a large number of basic amino acids (Table 1) and their cationic properties are thought to be important for cell membrane penetration (Futaki *et al.*, 2001; Chauhan *et al.*, 2007). Their positive charge, however, causes them to adsorb nonspecifically to negatively charged cell

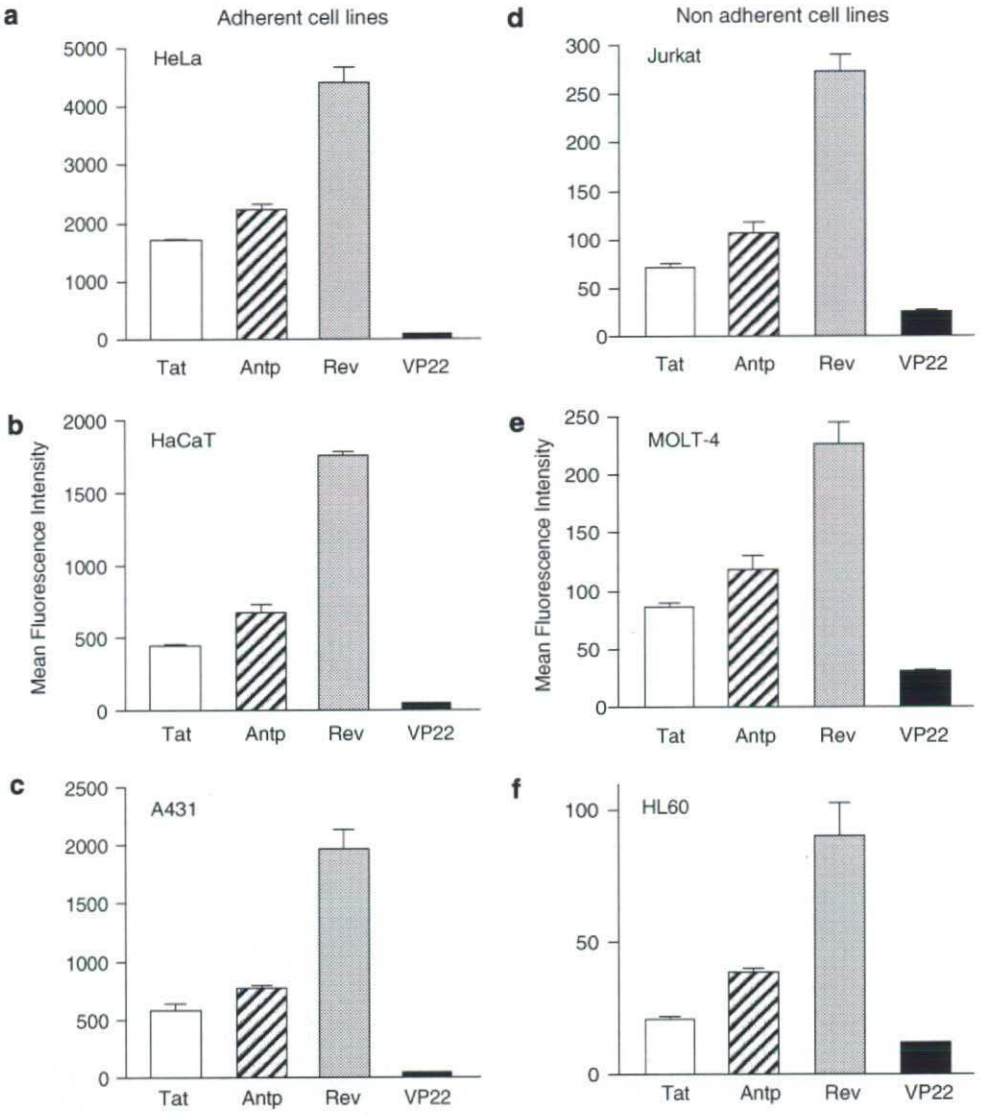

Figure 1 Comparison of the cellular uptake of protein transduction domains (PTDs). FAM-labelled Tat (white column), antennapedia (Antp; hatched column), Rev (grey column) and VP22 (black column) were incubated with six cell lines: HeLa (**a**), HaCaT (**b**), A431 (**c**), Jurkat (**d**), MOLT-4 (**e**) and HL60 (**f**) at 10 μM for 3 h. After trypsin treatment to digest PTDs adsorbed on the cell surface, the PTD-transduced cells were harvested and analysed by flow cytometry. Note that the *y* axis scales for the adherent cell lines are markedly different from that for the nonadherent cell lines. Data shown are the mean ± s.d. of triplicate assays.

membranes (Richard *et al.*, 2003). For this reason, the cells were treated with excess trypsin to eliminate nonspecific plasma membrane binding of the PTDs prior to measurement.

The relative order of their translocation efficiency (Rev > Antp > Tat > VP22), which was based on mean fluorescence, was independent of the cell type (that is, adherent or nonadherent). Furthermore, using PTD-fused Venus, we confirmed that Rev had the highest transduction efficiency (data not shown). Equally important, the overall translocation efficiency of the PTDs depended markedly on whether the cells were adherent (HeLa, HaCaT and A431 cells) or nonadherent (Jurkat, MOLT-4 and HL60 cells). The transduction efficiency was much higher in the adherent cell lines compared with the nonadherent cell lines (Figure 1); note that that the fluorescence (uptake) was about 8- to 25-fold greater in the adherent, than in nonadherent, cell lines.

The cytotoxic properties of the four PTDs were evaluated in adherent (HeLa) and nonadherent (Jurkat) cells. To assess the long-term changes in proliferation, mitochondrial dehydrogenase activity was measured using a WST-8 assay 24 h after PTD treatment. In HeLa cells, there was a remarkable decrease in cell viability when the cells were incubated with Antp at 100 μM, whereas other PTDs were not cytotoxic at the higher concentrations (Figure 2a). In contrast in Jurkat cells, Antp was extremely cytotoxic in a dose-dependent manner and Rev reduced cell proliferation by approximately 40% (Figure 2b). Previous reports indicated that amphipathic peptides, such as transportan, induced cytotoxicity by perturbing the cellular membrane (Hallbrink *et al.*, 2001; Jones *et al.*, 2005; Saar *et al.*, 2005; El-Andaloussi *et al.*, 2007). Thus, the membrane integrity of PTD-treated cells was also measured using an LDH leakage assay. Antp

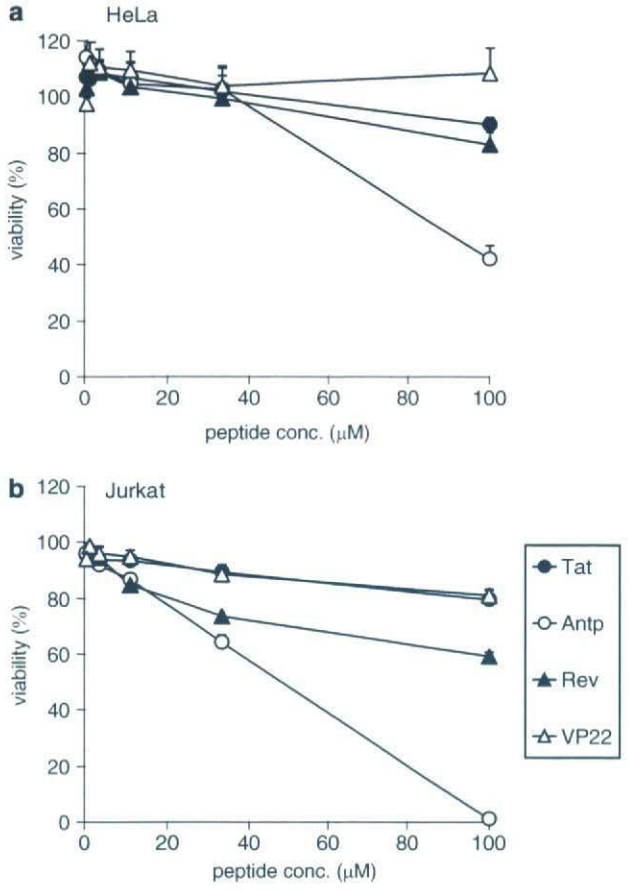

Figure 2 Viability of protein transduction domain (PTD)-treated cells. HeLa cells (**a**) and Jurkat cells (**b**) were incubated with serially diluted biotin-conjugated Tat, antennapedia (Antp), Rev and VP22 at 37 °C. After 24 h, cell viability was analysed using a WST-8 assay. Data shown are the mean ± s.d. of triplicate assays.

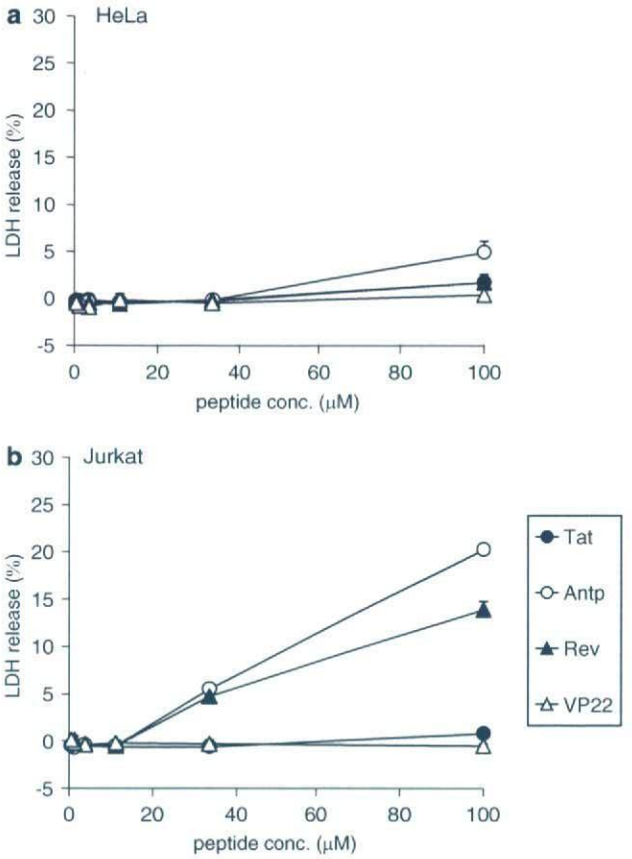

Figure 3 Membrane integrity of protein transduction domain (PTD)-treated cells. HeLa cells (**a**) and Jurkat cells (**b**) were incubated with serially diluted biotin-conjugated Tat, antennapedia (Antp), Rev and VP22 at 37 °C. After 3 h, the release of lactate dehydrogenase (LDH) was analysed. Data shown are the mean ± s.d. of triplicate assays.

and Rev induced significant LDH leakage in Jurkat cells, but only low LDH leakage was detected in Antp-treated HeLa cells (Figure 3). The membrane-perturbing effect of Antp and Rev contributed to the uptake of peptides, which are shown in Figure 1. Jurkat cells appear more sensitive to Antp or Rev treatment than HeLa cells; this difference in cytotoxicity and translocation efficiency may indicate a difference in the PTD-uptake mode.

Intracellular transduction mechanism of PTDs

The results of *in vitro* studies suggest that PTDs enter the cell via an energy-dependent endocytotic pathway (Lundberg *et al.*, 2003; Richard *et al.*, 2003). In particular, studies using various macropinocytosis inhibitors, such as methyl-β-cyclodextrin, to deplete cholesterol from the membrane (Grimmer *et al.*, 2002; Liu *et al.*, 2002), cytochalasin D, to inhibit F-actin elongation (Sampath and Pollard, 1991), or amiloride, to inhibit the Na^+-H^+ exchanger (West *et al.*, 1989), indicate that Tat is taken up into the cell via lipid raft-dependent macropinocytosis. To the best of our knowledge, however, few comparative studies have analysed the cellular uptake pathway of the four PTDs discussed in this paper. Therefore, we used flow cytometry analysis to determine whether PTD uptake is energy dependent or occurs via lipid raft-mediated macropinocytosis. First, we treated cells with PTD-FAM at 37 or 4 °C and then measured cell fluorescence (Figure 4). At 4 °C, transferrin, which enters cells by clathrin-dependent endocytosis (Schmid, 1997), inhibited the transduction efficiency compared with that at 37 °C. All four PTDs had low transduction ability at 4 °C, indicating that their cellular uptake was energy dependent. We next examined the PTD-FAM uptake efficiency in methyl-β-cyclodextrin-, cytochalasin D- and amiloride-treated HeLa cells. These cell treatments inhibited PTD-FAM incorporation in a dose-dependent manner, but transferrin was not affected (Figure 5). Furthermore, in HeLa cells treated with PTD-FAM, only punctuate fluorescence was observed using confocal laser scanning microscopic analysis (Figure 6). These results indicated that all the PTDs evaluated in this study enter the cell through the macropinocytotic pathway and that most of them were trapped in intracellular vesicles, the macropinosomes.

Intracellular localization of PTD–protein conjugates

We next examined the intracellular behaviour of the individual PTDs in more detail. To investigate whether

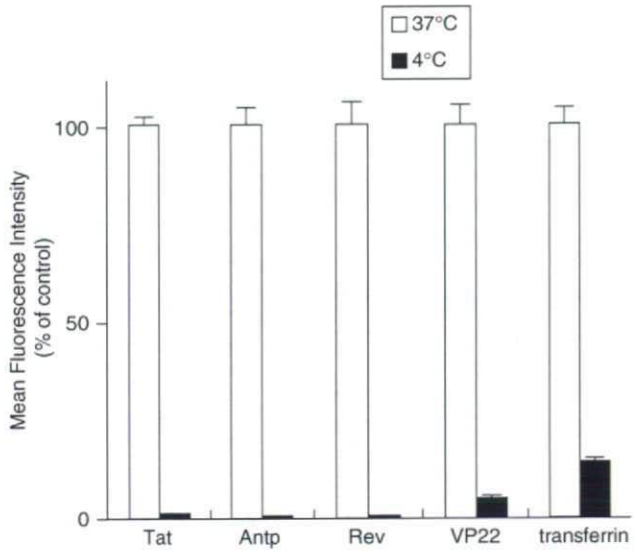

Figure 4 Effects of temperature on protein transduction domain (PTD) transduction efficiency. HeLa cells were preincubated at 37 or 4 °C for 1 h prior to adding FAM-labelled PTDs or fluorescein isothiocyanate-labelled transferrin for 3 h. Cells were washed in trypsin and analysed by flow cytometry. Data shown are the mean ± s.d. of triplicate assays.

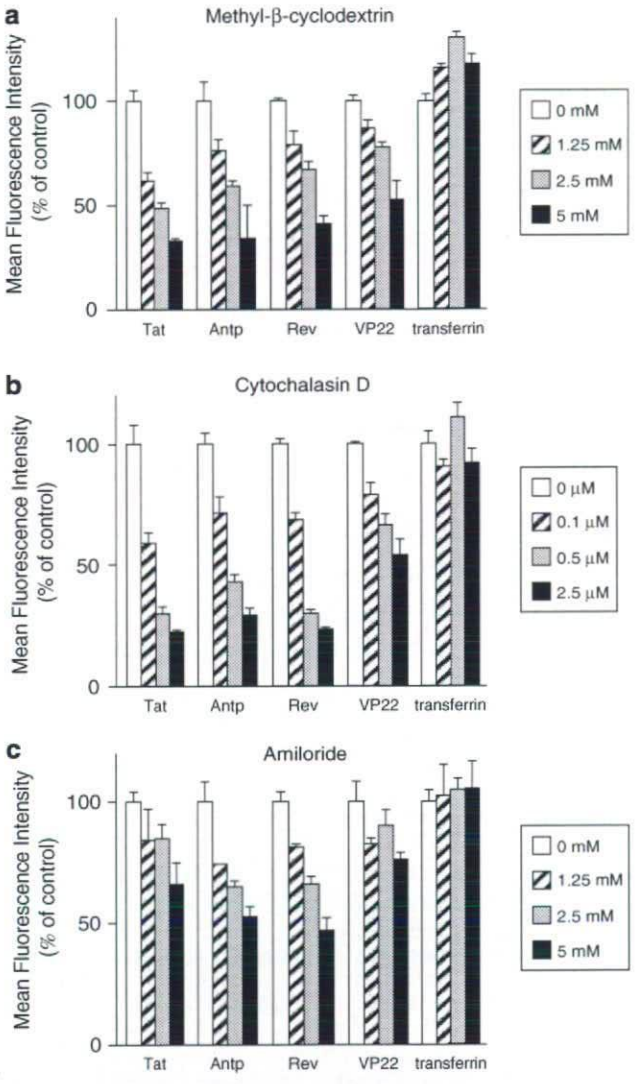

Figure 5 Effects of endocytosis inhibitors on transduction efficiency of protein transduction domains (PTDs). HeLa cells were pretreated with a range of concentrations of (**a**) methyl-β-cyclodextrin, (**b**) cytochalasin D or (**c**) amiloride for 30 min prior to adding FAM-labelled PTDs or fluorescein isothiocyanate-labelled transferrin for 1 h (**a** and **b**) or 30 min (**c**). Cells were washed in trypsin and analysed by flow cytometry. Data shown are the mean ± s.d. of triplicate assays.

individual PTDs are located in the same vesicles, we used Tat-fused HA2 peptide (HA2-Tat), an influenza virus-derived endosome-disrupting peptide. HA2-Tat improves the activity of Tat-fused Cre recombinase (Wadia *et al.*, 2004). Because HA2 alone cannot enter the cell, HA2-Tat is thought to enter the cell in a Tat-dependent manner and to disrupt the membrane of endosomal vesicles in which the Tat cargo is trapped. Thus, if Antp, Rev and VP22 are trapped in the same vesicles as Tat, the fluorescence should spread throughout the cytosol following cotreatment of the cells with HA2-Tat. As predicted, in HeLa cells cotreated with Antp-, Rev- or VP22-Venus and HA2-Tat, the Venus-derived fluorescence spread throughout the cytosol, whereas in the cells treated with Antp-, Rev- or VP22-Venus alone, only punctuate fluorescence was observed (Figure 7). These results suggested that all the PTDs evaluated in this study entered the cell through a macropinocytotic pathway and were trapped in the same vesicles as Tat.

Discussion

In the present study, we have systematically compared PTD-mediated molecular transduction mechanisms. Our findings indicated that individual PTDs have different levels of transduction efficiency and cytotoxicity, suggesting that PTDs are internalized into live cells via different mechanisms. We also examined the internalization pathway and intracellular localization of Tat, Antp, Rev and VP22. Unexpectedly, all the PTDs evaluated in this study entered the cell through the macropinocytotic pathway and were trapped in the same vesicles as Tat. The finding that the intracellular transduction pathways of the four PTDs were the same suggests that the method of cell internalization does not contribute to the differences in the PTD transduction efficiency or cytotoxicity. Although the reason for this phenomenon is not clear, we speculate that the primary structure of the individual PTDs or the cell surface proteins that interact with the individual PTDs contribute to the differences in their transduction efficiency and cytotoxicity.

The initial step in the mechanism of cellular entry of PTDs is thought to be the strong ionic interaction between the amino-acid residues of the PTDs and the plasma membrane constituents. Because the translocation is solely physically mediated, the charge distribution and amphipathicity of the peptide and its interaction with the plasma membrane is critical (Pujals *et al.*, 2006). Although most PTDs, if not all, contain a large number of basic amino acids, such as arginine or lysine, the theoretical isoelectric point (pI) value of each PTD used in this study was essentially identical (Tat, Antp,

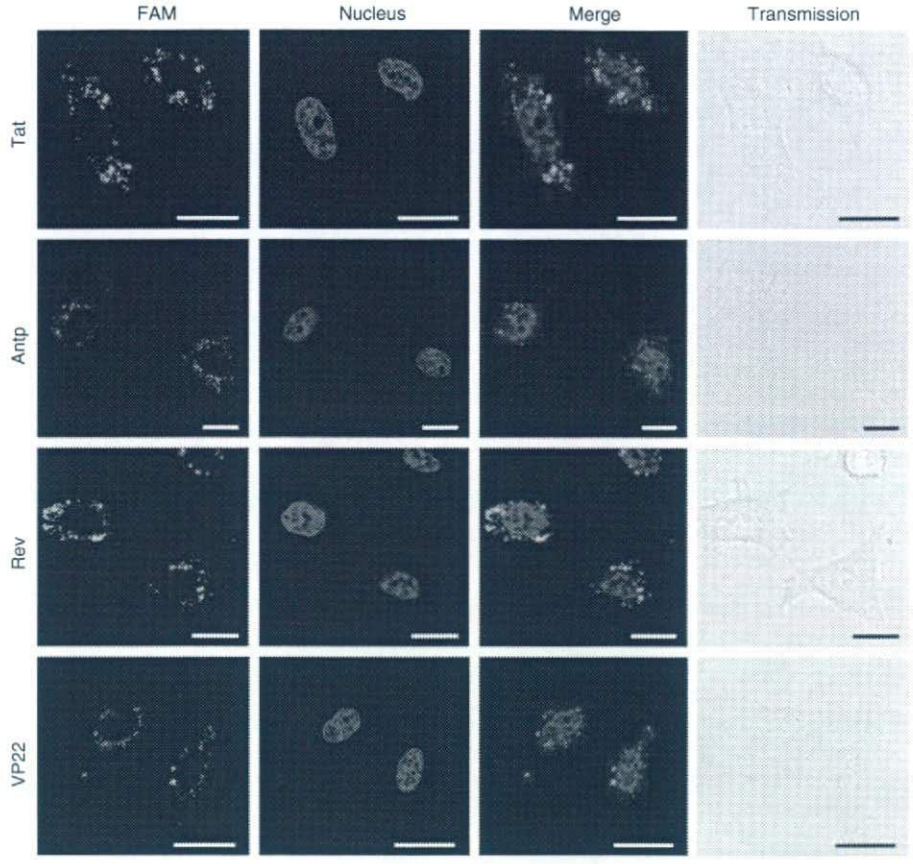

Figure 6 Intracellular behaviour of protein transduction domain (PTD)-FAM in living cells. HeLa cells were treated with 10 μM PTD-FAM for 3 h. Fluorescence images were acquired using confocal laser scanning microscopy and the signals were merged electronically. The nucleus was counterstained with Hoechst 33342 (blue). From top to bottom: Tat-, antennapedia (Antp)-, Rev- and VP22-FAM. From left to right: FAM (green), nucleus (blue), merged fluorescence and transmission image. Scale bars in each microphotograph indicate 20 μm.

Rev and VP22 have pI values of 12.70, 12.31, 12.60 and 12.01, respectively). Therefore, the internalization efficiency does not appear to depend on the cationic features of the PTDs.

The amphipathicity of the carrier is probably responsible not only for the strong interaction with the lipid membranes (Yandek *et al.*, 2007), but also for the disruption of the cellular membrane, which results in cell death (Hallbrink *et al.*, 2001; Jones *et al.*, 2005; Saar *et al.*, 2005; El-Andaloussi *et al.*, 2007). In terms of cytotoxicity, our data indicate that Antp and Rev both disrupt the membrane (Figure 3), but Rev does not contain an amphipathic structure. Furthermore, there was no correlation between hydrophobicity and transduction efficiency. Thus, differences in the PTD-mediated transduction efficiency and cytotoxicity might be due to the molecular weight or pI of the conjugated cargo.

The cellular events required for internalization, however, differ between reports and are often conflicting. The first mechanistic studies led to the proposal that PTD internalization occurs rapidly in a receptor- and energy-independent manner, perhaps by destabilizing the lipid bilayer or by the formation of inverted micelles with subsequent release of their contents within the intracellular space (Berlose *et al.*, 1996). More recently, an active mechanism based on vesicular uptake was proposed as the general mode of cell internalization of PTDs. In our experiment, although all four PTDs tended to be present in the same vesicles, the detailed mechanism for this colocalization is not yet known. It has been suggested that PTD internalization requires cell surface heparan sulphate proteoglycans (Tyagi *et al.*, 2001; Console *et al.*, 2003; Ziegler and Seelig, 2004). Because Tat interacts electrostatically with heparan sulphate proteoglycan present on the cell surface, it is possible that some PTDs are taken into the same vesicles when they interact with one heparan sulphate proteoglycan. In contrast, as shown in Figure 7, although fluorescence was observed throughout the cytosol, punctate fluorescence was also observed when the cells were cotreated with PTD-Venus and HA2-Tat. This finding suggested that the PTDs did not all exist in the same vesicles and that some PTDs entered the cell through another pathway. This is just speculation, however, and we are now using proteome analysis, such as liquid chromatography coupled with mass spectrometry or two-dimensional gel electrophoresis, to examine whether there are individual cell surface receptors for different PTDs.

In summary, our data suggest that Antp, Rev, VP22 and Tat cross the plasma membrane and reach the macropinosomes via different mechanisms. Our findings also indicate that several issues, such as endosome entrapment and low cell specificity, which limit the therapeutic activity of the cargo,

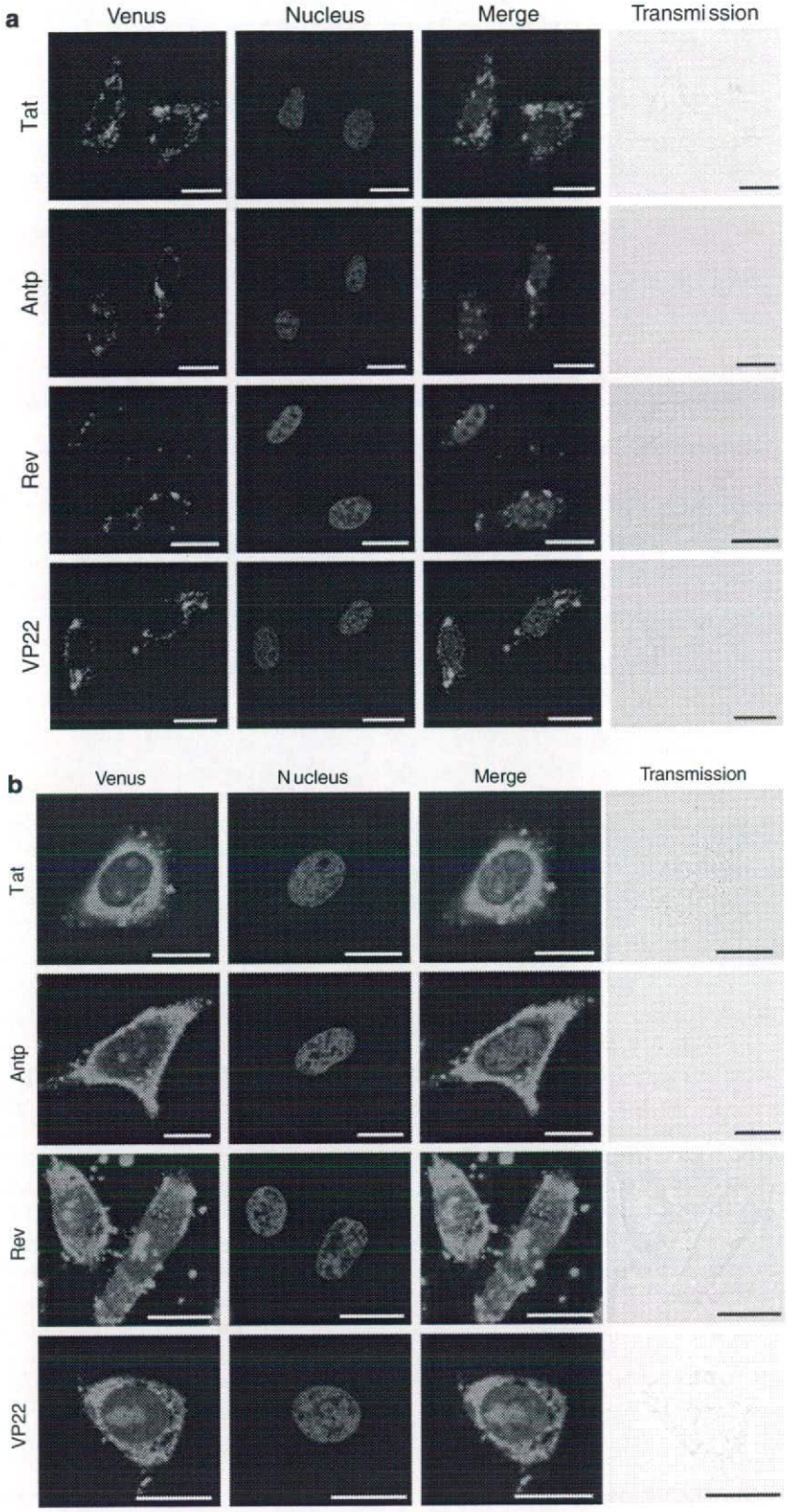

Figure 7 Intracellular behaviour of protein transduction domain (PTD)-Venus in living cells. HeLa cells were treated with 10 μM PTD-Venus alone (**a**) or 10 μM HA2-Tat (**b**) for 3 h. Fluorescence images were acquired using confocal laser scanning microscopy and the signals were merged electronically. The nucleus was counterstained with Hoechst 33342 (blue). From top to bottom: Tat-, antennapedia (Antp)-, Rev- and VP22-Venus. From left to right: Venus (green), nucleus (blue), merged fluorescence and transmission image. Scale bars in each microphotograph indicate 20 μm.

must be overcome before effective PTD-based drug delivery carriers can be fully developed. We previously reported that cotreatment with HA2-Tat enhances the cytosolic release of Tat-fused peptide-blockers and their biological activities, thereby overcoming the issue of endosome entrapment (Sugita *et al.*, 2007). Furthermore, although the transduction mechanism of PTDs is not yet well understood, these differences led us to explore the possibility of creating novel PTDs. We successfully created novel PTDs that have higher transduction efficiencies than Tat, using a unique phage display-based screening strategy that we previously developed (Mukai *et al.*, 2006; Kamada *et al.*, 2007). Moreover, based on our PTD-screening system, we are currently working to create more useful PTDs with cell type specificity.

Conflict of interest

The authors state no conflict of interest.

References

Berlose JP, Convert O, Derossi D, Brunissen A, Chassaing G (1996). Conformational and associative behaviours of the third helix of antennapedia homeodomain in membrane-mimetic environments. *Eur J Biochem* **242**: 372–386.

Borsello T, Forloni G (2007). JNK signalling: a possible target to prevent neurodegeneration. *Curr Pharm Des* **13**: 1875–1886.

Brusic V, Marina O, Wu CJ, Reinherz EL (2007). Proteome informatics for cancer research: from molecules to clinic. *Proteomics* **7**: 976–991.

Chauhan A, Tikoo A, Kapur AK, Singh M (2007). The taming of the cell penetrating domain of the HIV Tat: myths and realities. *J Control Release* **117**: 148–162.

Console S, Marty C, Garcia-Echeverria C, Schwendener R, Ballmer-Hofer K (2003). Antennapedia and HIV transactivator of transcription (TAT) 'protein transduction domains' promote endocytosis of high molecular weight cargo upon binding to cell surface glycosaminoglycans. *J Biol Chem* **278**: 35109–35114.

Derossi D, Joliot AH, Chassaing G, Prochiantz A (1994). The third helix of the Antennapedia homeodomain translocates through biological membranes. *J Biol Chem* **269**: 10444–10450.

Drabik A, Bierczynska-Krzysik A, Bodzon-Kulakowska A, Suder P, Kotlinska J, Silberring J (2007). Proteomics in neurosciences. *Mass Spectrom Rev* **26**: 432–450.

El-Andaloussi S, Jarver P, Johansson HJ, Langel U (2007). Cargo dependent cytotoxicity and delivery efficacy of cell-penetrating peptides: a comparative study. *Biochem J* **407**: 285–292.

Elliott G, O'Hare P (1997). Intercellular trafficking and protein delivery by a herpesvirus structural protein. *Cell* **88**: 223–233.

Ferrari A, Pellegrini V, Arcangeli C, Fittipaldi A, Giacca M, Beltram F (2003). Caveolae-mediated internalization of extracellular HIV-1 tat fusion proteins visualized in real time. *Mol Ther* **8**: 284–294.

Fittipaldi A, Ferrari A, Zoppe M, Arcangeli C, Pellegrini V, Beltram F *et al.* (2003). Cell membrane lipid rafts mediate caveolar endocytosis of HIV-1 Tat fusion proteins. *J Biol Chem* **278**: 34141–34149.

Futaki S, Suzuki T, Ohashi W, Yagami T, Tanaka S, Ueda K *et al.* (2001). Arginine-rich peptides. An abundant source of membrane-permeable peptides having potential as carriers for intracellular protein delivery. *J Biol Chem* **276**: 5836–5840.

Grimmer S, van Deurs B, Sandvig K (2002). Membrane ruffling and macropinocytosis in A431 cells require cholesterol. *J Cell Sci* **115**: 2953–2962.

Hallbrink M, Floren A, Elmquist A, Pooga M, Bartfai T, Langel U (2001). Cargo delivery kinetics of cell-penetrating peptides. *Biochim Biophys Acta* **1515**: 101–109.

Han X, Bushweller JH, Cafiso DS, Tamm LK (2001). Membrane structure and fusion-triggering conformational change of the fusion domain from influenza hemagglutinin. *Nat Struct Biol* **8**: 715–720.

Hawiger J (1999). Noninvasive intracellular delivery of functional peptides and proteins. *Curr Opin Chem Biol* **3**: 89–94.

Joliot A, Prochiantz A (2004). Transduction peptides: from technology to physiology. *Nat Cell Biol* **6**: 189–196.

Jones SW, Christison R, Bundell K, Voyce CJ, Brockbank SM, Newham P *et al.* (2005). Characterisation of cell-penetrating peptide-mediated peptide delivery. *Br J Pharmacol* **145**: 1093–1102.

Kamada H, Okamoto T, Kawamura M, Shibata H, Abe Y, Ohkawa A *et al.* (2007). Creation of novel cell-penetrating peptides for intracellular drug delivery using systematic phage display technology originated from Tat transduction domain. *Biol Pharm Bull* **30**: 218–223.

Kaplan IM, Wadia JS, Dowdy SF (2005). Cationic TAT peptide transduction domain enters cells by macropinocytosis. *J Control Release* **102**: 247–253.

Liu NQ, Lossinsky AS, Popik W, Li X, Gujuluva C, Kriederman B *et al.* (2002). Human immunodeficiency virus type 1 enters brain microvascular endothelia by macropinocytosis dependent on lipid rafts and the mitogen-activated protein kinase signaling pathway. *J Virol* **76**: 6689–6700.

Lundberg M, Wikstrom S, Johansson M (2003). Cell surface adherence and endocytosis of protein transduction domains. *Mol Ther* **8**: 143–150.

Mukai Y, Sugita T, Yamato T, Yamanada N, Shibata H, Imai S *et al.* (2006). Creation of novel protein transduction domain (PTD) mutants by a phage display-based high-throughput screening system. *Biol Pharm Bull* **29**: 1570–1574.

Murriel CL, Dowdy SF (2006). Influence of protein transduction domains on intracellular delivery of macromolecules. *Expert Opin Drug Deliv* **3**: 739–746.

Nagahara H, Vocero-Akbani AM, Snyder EL, Ho A, Latham DG, Lissy NA *et al.* (1998). Transduction of full-length TAT fusion proteins into mammalian cells: TAT-p27Kip1 induces cell migration. *Nat Med* **4**: 1449–1452.

Nori A, Kopecek J (2005). Intracellular targeting of polymer-bound drugs for cancer chemotherapy. *Adv Drug Deliv Rev* **57**: 609–636.

Pujals S, Fernandez-Carneado J, Lopez-Iglesias C, Kogan MJ, Giralt E (2006). Mechanistic aspects of CPP-mediated intracellular drug delivery: relevance of CPP self-assembly. *Biochim Biophys Acta* **1758**: 264–279.

Rhodes DR, Chinnaiyan AM (2005). Integrative analysis of the cancer transcriptome. *Nat Genet* **37** (Suppl): S31–S37.

Richard JP, Melikov K, Brooks H, Prevot P, Lebleu B, Chernomordik LV (2005). Cellular uptake of unconjugated TAT peptide involves clathrin-dependent endocytosis and heparan sulfate receptors. *J Biol Chem* **280**: 15300–15306.

Richard JP, Melikov K, Vives E, Ramos C, Verbeure B, Gait MJ *et al.* (2003). Cell-penetrating peptides. A reevaluation of the mechanism of cellular uptake. *J Biol Chem* **278**: 585–590.

Rojas M, Donahue JP, Tan Z, Lin YZ (1998). Genetic engineering of proteins with cell membrane permeability. *Nat Biotechnol* **16**: 370–375.

Saar K, Lindgren M, Hansen M, Eiriksdottir E, Jiang Y, Rosenthal-Aizman K *et al.* (2005). Cell-penetrating peptides: a comparative membrane toxicity study. *Anal Biochem* **345**: 55–65.

Sampath P, Pollard TD (1991). Effects of cytochalasin, phalloidin, and pH on the elongation of actin filaments. *Biochemistry* **30**: 1973–1980.

Schmid SL (1997). Clathrin-coated vesicle formation and protein sorting: an integrated process. *Annu Rev Biochem* **66**: 511–548.

Schwarze SR, Ho A, Vocero-Akbani A, Dowdy SF (1999). *In vivo* protein transduction: delivery of a biologically active protein into the mouse. *Science* **285**: 1569–1572.

Schwarze SR, Hruska KA, Dowdy SF (2000). Protein transduction: unrestricted delivery into all cells? *Trends Cell Biol* **10**: 290–295.

Skehel JJ, Cross K, Steinhauer D, Wiley DC (2001). Influenza fusion peptides. *Biochem Soc Trans* **29**: 623–626.

Sugita T, Yoshikawa T, Mukai Y, Yamanada N, Imai S, Nagano K *et al.* (2007). Improved cytosolic translocation and tumor-killing

A thorough understanding of the biology of the TNF/TNFR system is a prerequisite to the safe and effective development of anti-TNF therapeutics. In particular, several factors and mechanisms hypothesized to be involved in the side effects elicited by anti-TNF drugs need to be tested (Curtis et al., 2007; Jacobs et al., 2007; Schneeweiss et al., 2007). These include the differential power of the drugs to neutralize TNF bioavailability and the differential inhibition of TNF signaling events. Despite extensive studies on the molecular biology of TNF/TNFR1 signaling (Micheau and Tschopp, 2003) the functions of TNFR2 are poorly understood. There is an increasing need for a comprehensive understanding of TNF/TNFR2 biology, particularly in terms of the development of TNFR-selective drugs.

In this context, we have used a novel phage-display based screening system (Yamamoto et al., 2003; Shibata et al., 2004, 2008) to develop structural mutants of TNF to help clarify the biology of TNF/TNFR2 interactions. These TNF variants, which exert TNFR2-mediated agonistic or antagonistic activity, might be extremely valuable for elucidating structure-activity relationships between TNF and TNFR2. So far, in order to evaluate the bioactivity of TNF through TNFR2, many researchers have used the TNFR2 over-expressing cell lines (Heller et al., 1992; Weiss et al., 1998), such as rat/mouse T hybridomas transfected with human TNFR2 (PC60-hR2) (Vandenabeele et al., 1992). The PC60-hR2 assay is based on granulocyte macrophage colony-stimulating factor (GM-CSF) secretion mediated by TNF/TNFR2 stimuli. The GM-CSF secretion level is quantified by proliferation of GM-CSF-dependent cell lines or by ELISA. However, this two-step assay system is complicated and the screening process is highly laborious. Thus, there are increasing demands for the development of a simple, highly sensitive screening system that is TNFR2-selective.

In the present study, we developed a simple but highly sensitive cell death-based assay system for evaluating TNFR2-mediated activity. We constructed a lentiviral vector expressing a chimeric receptor derived from the extracellular (EC) and transmembrane (TM) domain of human TNFR2 (hTNFR2) and the intracellular (IC) domain of mouse Fas (mFas). Additionally, to eliminate the influence of the endogenous TNFR1, the chimeric receptor was expressed on $TNFR1^{-/-}R2^{-/-}$ preadipocytes (Xu et al., 1999). We found that hTNFR2/mFas-expressing preadipocyte (hTNFR2/mFas-PA) showed about 80-times higher sensitivity after treatment with soluble-TNF and over the conventional method. Furthermore, hTNFR2/mFas-PA could detect not only transmembrane TNF- (tmTNF) but also soluble TNF-activity. The technology described herein will be highly useful both as an assay system for various TNF variants *via* TNFR2 and also as a cell-based drug discovery system for TNFR2 agonists/antagonists.

2. Materials and methods

2.1. Cell culture

$TNFR1^{-/-}R2^{-/-}$, $TNFR1^{-/-}$, and wild-type (wt) preadipocytes established from day 16–17 mouse embryos were generously provided by Dr. Hotamisligil (Harvard School of Public Health, Boston MA). Preadipocytes, 293T cells and HeLaP4 cells were cultured in Dulbecco's modified Eagle's medium (DMEM; Sigma-Aldrich, Inc., Tokyo, Japan) with 10% bovine fetal serum (FBS) and 1% antibiotic cocktail (penicillin 10,000 u/ml, streptomycin 10 mg/ml, and amphotericin B 25 μg/ml; Nacalai Tesque, Kyoto, Japan). The rat/mouse T hybridomas PC60-hR2 cells (hTNFR2 transfected PC60 cells) were generously provided by Dr. Vandenabeele (University of Gent, Belgium) and cultured in RPMI 1640 (Sigma-Aldrich, Inc.) with 10% FBS, 1 mM sodium pyrubate, 5×10^{-5} M 2-ME, 3 μg/ml puromycin (Wako Pure Chemical Industries, Osaka, Japan), and 1% antibiotic cocktail. $TNFR1^{-/-}R2^{-/-}$ mouse macrophages were generously provided by Dr. Aggarwal (University of Texas MD Anderson Cancer Center, Houston, TX), and cultured in RPMI 1640 with 10% FBS and 1% antibiotic cocktail.

2.2. Construction of self-inactivating (SIN) lentiviral vector

Vectors were constructed using standard cloning procedures. A DNA fragment encoding the EC and TM parts of hTNFR2 was amplified by polymerase chain reaction (PCR) from human peripheral blood lymphocyte cDNA with the following primer pairs: forward primer (5′-GAT TAC GCC AAG CTT GTC GAC CAC CAT GGC GCC CGT CGC CGT CTG GGC CGC GCT GGC CGT CGG ACT GGA G-3′) containing a SalI site at the 5′-end and a reverse primer (5′-CAC CTT GGC TTC TCT CTG CTT TCG AAG GGG CTT CTT TTT CAC CTG GGT CA-3′) containing a Csp45I site. The resulting amplified fragment was subcloned into pCR-Blunt II-TOPO (Invitrogen Corp., Carlsbad, CA) to generate pCR-Blunt-hTNFR2. A fragment encoding the IC domain of mFas was amplified by PCR from mouse spleen cDNA with the following primer pair: forward primer (5′-AAT TCC ACT TGT ATT TAT ACT TCG AAA GTA CCG GAA AAG A-3′) containing a Csp45I site and a reverse primer (5′-GTC ATC CTT GTA GTC TGC GGC CGC TCA CTC CAG ACA TTG TCC TTC ATT TTC ATT TCC A-3′) containing a NotI site at the 5′-end. The mFas DNA fragment was subcloned into pCR-Blunt-hTNFR2 between the Csp45I and NotI sites to combine the EC and TM domains of hTNFR2 to the IC domains of mFas, generating pCR-Blunt-hTNFR2/mFas (Fig. 1A). Then the hTNFR2/mFas DNA fragment was cloned between the XhoI and NotI sites of SIN lentiviral vector construct, which contains the blasticidin (Bsd) resistance gene, generating CSII-CMV-hTNFR2/mFas-IRES2-Bsd (Fig. 1B). For construct tmTNF, a DNA fragment encoding non-cleavable human tmTNF h(tmTNFΔ1-12), generated by deleting amino acids 1–12 in the N-terminal part of hTNF, was amplified by PCR from hTNF cDNA with following primer pair: forward primer (5′-AGT GAT CGG CCC CCA GAG GGA AGC TTA GAT CTC TCT CTA ATC AGC CCT CTG GCC CAG GCA GTA GCC CAT GTT GTA GCA AAC CCT CAA G-3′) and reverse primer (5′-GGT TGG ATG TTC GTC CTC CGC GGC CGC CTA ACT AGT TCA CAG GGC AAT GAT CCC AAA GTA GAC CTG-3′) and cloned into the pY03′ vector. Then tmTNFΔ1–12 DNA fragment was cloned between the SalI and XhoI sites of the SIN vector construct, generating CSII-EF-tmTNF-IRES-GFP.

2.3. Preparation of lentiviral vectors

The method used to prepare the lentiviral vector has been described previously (Miyoshi et al., 1999; Katayama et al.,

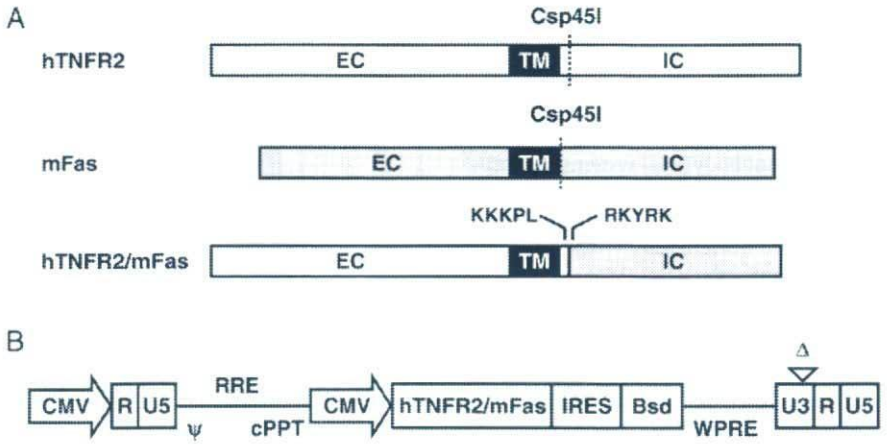

Fig. 1. Construction of hTNFR2/mFas chimeric receptor gene and vector. (A) The cDNA structures of hTNFR2, mFas and fusion genes (hTNFR2/mFas) are shown. EC: extracellular domain, TM: transmembrane domain, IC: Intracellular domain. (B) Schematic representation of self-inactivating (SIN) LV plasmid (CSII-CMV-hTNFR2/mFas-IRES-Bsd). CMV, cytomegalovirus promoter; ψ: packaging signal; RRE, rev responsive element; cPPT, central polypurine tract; IRES, Encephalomyocarditis virus internal ribosomal entry site; Bsd, Blasticidin; WPRE, woodchuck hepatitis virus posttranscriptional regulatory element. Δ: deleting 133 bp in the U3 region of the 3′ long terminal repeat.

2004). In brief, 293T cells were transfected by the calcium phosphate method with three plasmids: packaging construct (pCAG-HIVgp), VSV-G and Rev expressing construct (pCMV-VSV-G-RSV-Rev) and SIN vector construct (CSII-CMV-TNFR2/Fas-IRES2-Bsd or CSII-EF-tmTNF-IRES-GFP). Two days after transfection, the conditioned medium was collected and the virus was concentrated by ultracentrifugation at 50,000 × g for 2 h at 20 °C. The pelleted virus was resuspended in Hanks' balanced salt solution (GIBCO BRL, Paisley, UK). Vector titers were determined by measuring the infectivity of HeLaP4 cells with serial dilutions of vector stocks using flow cytometric analysis (FCM) for hTNFR2/mFas- or GFP-positive cells.

2.4. Preparation of hTNFR2/mFas- or tmTNF-expressing cell culture

To prepare the hTNFR2/mFas- or tmTNF-expressing cell culture, $TNFR1^{-/-}R2^{-/-}$ preadipocytes or $TNFR1^{-/-}R2^{-/-}$ macrophages were infected with each lentiviral vector at a multiplicity of infection (MOI) of 100. Stable hTNFR2/mFas-transfectants were selected for growth in culture medium containing 8 μg/ml Bsd (Invitrogen Corp.) for 1 week. Expression of hTNFR2/mFas chimeric receptor on Bsd-resistant cells was detected by staining with biotinylated anti-hTNFR2 antibody (BD Biosciences, Franklin Lakes, NJ) at 0.5 μg/5×10^5 cells for 30 min at 4 °C. Subsequently, the cells were washed and stained with streptavidin-PE conjugate (BD Biosciences). The cell suspension was centrifuged at 800 × g, washed with PBS, centrifuged again, and then re-suspended in 500 μl of 0.4% paraformaldehyde. Fluorescence was analyzed on a FACS Vantage flow cytometer, and data were analyzed using CellQuest software (both BD Biosciences). The hTNFR2/mFas-positive cell cultures were used in subsequent experiments as hTNFR2/mFas-PA cells. For preparation of tmTNF-expressing $TNFR1^{-/-}R2^{-/-}$ macrophages (tmTNF-Mφ), IRES-driven GFP positive cells were sorted by FACSAria (BD Biosciences).

2.5. Cytotoxicity assays

Cells were seeded on 96-well micro titer plates at a density of 1.5×10^4 cells/well in culture medium. Serial dilutions of mouse or human TNF (mTNF or hTNF; Peprotech, Rocky Hill, NJ), anti-mFas antibody (clone Jo2; BD Biosciences), or paraformaldehyde-fixed tmTNF-Mφ were prepared with DMEM containing 1 μg/ml cycloheximide, and added to each well. After 48 h incubation, the cell viability was measured by WST-8 assay kit (Nacalai Tesque) according to the manufacturer's instructions. The assay is based on cleavage of the tetrazolium salt WST-8 to formazan by cellular mitochondrial dehydrogenase.

2.6. Induction of GM-CSF secretion on PC60-hR2

5×10^4 of PC60-hR2 cells were seeded on a 96 well plate and then exposed to a serial dilution of hTNF in the presence of IL-1β (2 ng/ml). After 24 h incubation, hTNFR2-mediated GM-CSF secretion on PC60-hR2 cells was quantified by ELISA kit according to the manufacturer's protocol (R&D Systems, Minneapolis, MN).

2.7. Immunoprecipitation and western blotting

For immunoprecipitation we used FLAG-TNF (a FLAG-tag fusion protein of hTNF), which was generated in *E. coli* and purified in our laboratory. The protocol for the expression and purification of recombinant proteins has been described previously (Yamamoto et al., 2003). 1×10^7 hTNFR2/mFas-PA cells were treated with or without 100 ng/ml of FLAG-TNF for 30 min at 37 °C. Cells were then harvested and lysed in 1 ml of lysis buffer (50 mM Tris HCl, pH 7.4, 150 mM NaCl, 1% Triton X-100, 1 mM EDTA and protease inhibitor cocktail; Sigma-Aldrich Inc.) and gently rocked at 4 °C for 30 min. Cell debris was removed by centrifugation at 10,000 ×g for 30 min. The resulting supernatant was immunoprecipitated with anti-FLAG-M2 affinity beads (Sigma, St.Louis, MO) for 4 h at 4 °C. Immune complexes bound to the beads were washed three

3.2. hTNFR2-expression analysis of LV-hTNFR2/mFas-Bsd infected Bsd-resistant cells

Using the LV technique followed by Bsd selection, we established transfectants that stably expressed hTNFR2/mFas chimeric receptor in which the EC and TM portion of hTNFR2 (amino acids 1–292) was fused to the IC region of mFas (amino acids 187–328) (Figs. 1A and B). FCM analysis revealed that almost 95% of Bsd-resistant cells expressed the EC domain of hTNFR2 (Fig. 3A). To determine whether hTNFR2/mFas retained binding activity against hTNF, we next performed immunoprecipitation and western blot analysis (Fig. 3B). These analyses showed that FLAG-TNFs were immunoprecipitated and eluted with hTNFR2/mFas from LV-transfected and Bsd-resistant cells, but not from parental TNFR1$^{-/-}$R2$^{-/-}$ preadipocytes and untreated cells. Thus, we succeeded in constructing hTNFR2/mFas expressing TNFR1$^{-/-}$ R2$^{-/-}$ preadipocytes that retained the ability to bind hTNF.

3.3. Induction of apoptosis on hTNFR2/mFas-PA

To examine whether the death signal could be transduced by stimulating the chimeric receptors, we evaluated the cell viability of soluble hTNF-treated hTNFR2/mFas-PA. As anticipated, addition of hTNF to hTNFR2/mFas-PA induced a strong cytotoxic effect 24 and 48 h later, whereas no cell death was detected using parental TNFR1$^{-/-}$R2$^{-/-}$ preadipocytes (Figs. 4A and B). After 48 h, more than 90% of hTNFR2/mFas-PA cells were killed by hTNF at a concentration of 4 ng/ml, resulting in a median effective concentration (EC50) of 250 pg/ml. The images in Figs. 4C and D show that hTNFR2/mFas-PA cells underwent clear morphological changes, indicating apoptosis by hTNF stimuli. Additionally, PC60-hR2 cells were tested for hTNFR2-mediated GM-CSF secretion (Fig. 4E). The concentration required to induce 50% of maximal secretion of GM-CSF obtained with hTNF (EC50) was approximately 20 ng/ml. Importantly, our bioassay based on cell death phenotype displayed a ~80-fold higher level of sensitivity over conventional methodologies. Moreover, tmTNF (Fig. 5) and anti-TNFR2 agonistic antibody (data not shown) induced hTNFR2/mFas-PA cell death.

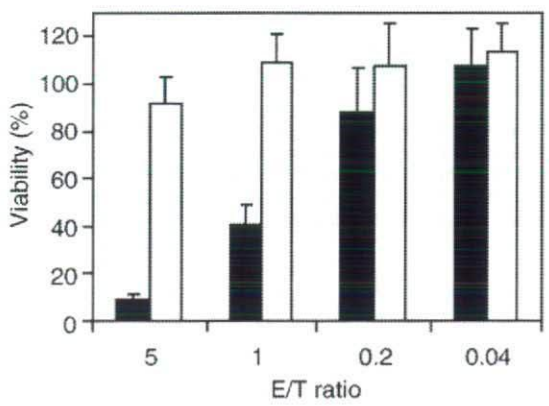

Fig. 5. hTNFR2/mFas-PA cells could be induced cell death by tmTNF. hTNFR2/mFas-PA cells were co-incubated with paraformaldehyde-fixed tmTNF-MΦ (filled bars) or TNFR1$^{-/-}$R2$^{-/-}$ MΦ (open bars) at an effector/target (E/T) ratio of 5:1, 1:1, 0.2:1 and 0.4:1 in the presence of cycloheximide (1 μg/ml). After 48 h, cell viability was measured by WST-8 Assay. Each data point represents the mean ± SD of triplicate measurements.

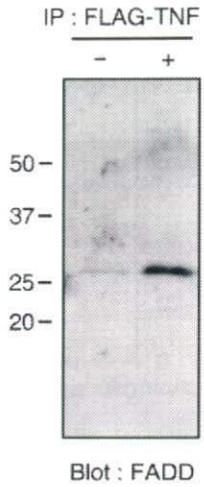

Fig. 6. Recruitment of FADD to the hTNFR2/mFas chimeric receptor in response to hTNF. hTNFR2/mFas-PA or TNFR1$^{-/-}$R2$^{-/-}$ cells were treated (+) with FLAG-TNF; (–) denotes untreated cells. Immunoprecipitation was performed with anti-FLAG antibody M2-conjugated beads. After extensive washing, immunocomplexes were eluted with 3×FLAG peptide. The eluted proteins were resolved on 10–20% SDS-PAGE gels and the presence of hTNFR2/mFas in the complex was detected by western blot using anti-FADD Antibody.

3.4. Recruitment of FADD to the hTNFR2/mFas chimeric receptor

Recent studies indicate that some TNFR family members, including Fas, self-associate as trimers prior to ligand binding. Activation of the pre-associated receptors is triggered by ligand-induced rearrangement of the assembled trimers (Algeciras-Schimnich et al., 2002). We speculated that the first reaction after ligand-induced oligomerization of hTNFR2/mFas might be the recruitment of FADD, leading to caspase-8 activation. To investigate the composition of the ligand-hTNFR2/mFas signaling complex, we treated hTNFR2/mFas-PA cells with FLAG-tagged hTNF and affinity purified the receptor complex using anti-FLAG antibody-conjugated beads, followed by western blot analysis with antibody against FADD. As expected, FADD was immunoprecipitated with hTNFR2/mFas on hTNF-treated hTNFR2/mFas-PA (Fig. 6). In similar experiments, we could not detect TRADD, which is recruited to TNFR1 in a ligand-dependent process (data not shown). It has been reported that, in contrast to TNFR1, Fas does not interact with TRADD but directly recruits FADD, leading to efficient cell death (Stanger et al., 1995; Dempsey et al., 2003). Because hTNFR2/mFas interacts with FADD, our hTNFR2/mFas-PA cell-based assay system will be useful for evaluating hTNF activity specifically *via* hTNFR2.

4. Discussion

Here, we developed a hTNFR2/mFas-PA cell-based assay system in order to investigate hTNF activity through hTNFR2. The assay is simple to perform and can detect hTNF-mediated hTNFR2 activity with high sensitivity. Because the hTNFR2/

mFas-PA system was engineered in TNFR1$^{-/-}$R2$^{-/-}$ preadipocytes, we were able to analyze hTNF-mediated hTNFR2 activity without affecting TNFR1-related apoptosis. Moreover, not only tmTNF- but also soluble TNF-mediated hTNFR2 activity was detectable using the hTNFR2/mFas-PA cell system.

In our system, hTNFR2-mediated cytotoxic activity on hTNFR2/mFas-PA cells was quantitatively determined using the WST-8 assay. Alternative methods, such as the MTT assay or Methylene Blue assay, are also capable of detecting cytotoxicity. Using the WST-8 assay, hTNFR2-mediated cytotoxic activity was readily detected 24 h after hTNF treatment (Fig. 4A), although a stronger signal was generated with a longer incubation time (48 h; Fig. 4B). Therefore, 48 h-treatment might be more appropriate for evaluating the activity of a low dose of hTNF or when analyzing an activity-weakened mutant TNF. Furthermore, if you evaluate in the absence of CHX, it may be desirable to alter the cell numbers from 1.5 to 1.0×10^4 cells/well. Previously, a similar assay system to the one described in this report was developed by Heidenreich et al. based on murine TNFR1$^{-/-}$R2$^{-/-}$ cells, which heterogenetically expressed human Fas conjugated with hTNFR2 (termed MF-R2-Fas cells) (Krippner-Heidenreich et al., 2002). However, there are some important differences between the MF-R2-Fas cells and the cell line used in our assay system (hTNFR2/mFas-PA), such as detachability. Surprisingly, unlike MF-R2-Fas cells, hTNFR2/mFas-PA cells can detect tmTNF-mediated activity as well as soluble TNF activity. Currently, the reason for this difference is unclear, although it may be caused by heterogeneity of the Fas domain. Indeed, the genetic homology between murine Fas and human Fas in IC domain is approximately 50%. Additionally, other factors may account for the observed differences between the two assay systems, such as expression level of the chimeric receptor. At any event, our results suggest that hTNFR2/mFas-PA cells will be useful in providing the basis for a highly sensitive assay system for analyzing hTNFR2 activity mediated by both soluble TNF and tmTNF. We are currently attempting to generate a TNFR2-selective mutant TNF using this assay system and a phage display system for TNF-therapy or anti-TNF therapy (unpublished data). We chose to use hTNFR2/mFas-PA cells in the screening process for a TNFR2-selective mutant TNF because this cell line is sensitive against not only purified TNF but also culture supernatants of TNF-transfected *E. coli* (crude samples). Therefore, our simple and sensitive bioassay enables high-throughput screening for TNFR2-selective mutant TNFs. The TNFR2-selective mutant will make it possible to perform a structure-function study of TNF/TNFR at any stage of function.

With the success of the human genome project, the focus of life science research has shifted to functional and structural analyses of proteins, such as disease proteomics (Oh et al., 2004; Gilchrist et al., 2006). Thus, there is increasing expectation on drug discovery/development based on the information from genomics or proteomics research, structural biology studies, or receptor-ligand interaction analyses. In particular, the therapeutic application of bioactive proteins, such as cytokines and the newly identified ligand proteins, is eagerly awaited (Gollob et al., 2003; Ansell et al., 2006). Surprisingly, however, these ligand proteins display multiple functions, which has severely limited their clinical application (Margolin et al., 1994; Eskander et al., 1997). Because the reason behind this limitation is that these ligand proteins stimulate different signal transduction pathways via multiple (two or more) receptors, the discovery of receptor-specific agonistic or antagonistic drugs is keenly awaited. Our assay system using a chimeric receptor strategy is applicable to other cytokines and thereby provides a new avenue for identifying receptor-specific agonists or antagonists. We fully anticipate that our novel technology will accelerate the development of TNFR2-related therapeutic molecules as well as acting as a research tool for studying the biology of TNFR2.

Acknowledgements

This study was supported in part by Grants-in-Aid for Scientific Research (No. 18015055, 17689008) from the Ministry of Education, Culture, Sports, Science and Technology of Japan, in part by Health Labor Sciences Research Grant from the Ministry of Health, Labor and Welfare of Japan, in part by Health Sciences Research Grants for Research on Health Sciences focusing on Drug Innovation from the Japan Health Sciences Foundation, and in part by JSPS Research Fellowships for Young Scientists from the Japan Society for the Promotion of Science.

References

Aggarwal, B.B., 2003. Signalling pathways of the TNF superfamily: a double-edged sword. Nat. Rev. Immunol. 3, 745.

Algeciras-Schimnich, A., Shen, L., Barnhart, B.C., Murmann, A.E., Burkhardt, J.K., Peter, M.E., 2002. Molecular ordering of the initial signaling events of CD95. Mol. Cell Biol. 22, 207.

Ansell, S.M., Geyer, S.M., Maurer, M.J., Kurtin, P.J., Micallef, I.N., Stella, P., Etzell, P., Novak, A.J., Erlichman, C., Witzig, T.E., 2006. Randomized phase II study of interleukin-12 in combination with rituximab in previously treated non-Hodgkin's lymphoma patients. Clin. Cancer Res. 12, 6056.

Ashkenazi, A., Dixit, V.M., 1998. Death receptors: signaling and modulation. Science 281, 1305.

Brown, S.L., Greene, M.H., Gershon, S.K., Edwards, E.T., Braun, M.M., 2002. Tumor necrosis factor antagonist therapy and lymphoma development: twenty-six cases reported to the Food and Drug Administration. Arthritis Rheum. 46, 3151.

Curtis, J.R., Patkar, N., Xie, A., Martin, C., Allison, J.J., Saag, M., Shatin, D., Saag, K.G., 2007. Risk of serious bacterial infections among rheumatoid arthritis patients exposed to tumor necrosis factor alpha antagonists. Arthritis Rheum. 56, 1125.

Dempsey, P.W., Doyle, S.E., He, J.Q., Cheng, G., 2003. The signaling adaptors and pathways activated by TNF superfamily. Cytokine Growth Factor Rev. 14, 193.

Devin, A., Cook, A., Lin, Y., Rodriguez, Y., Kelliher, M., Liu, Z., 2000. The distinct roles of TRAF2 and RIP in IKK activation by TNF-R1: TRAF2 recruits IKK to TNF-R1 while RIP mediates IKK activation. Immunity 12, 419.

Eskander, E.D., Harvey, H.A., Givant, E., Lipton, A., 1997. Phase I study combining tumor necrosis factor with interferon-alpha and interleukin-2. Am. J. Clin. Oncol. 20, 511.

Feldmann, M., Maini, R.N., 2003. Lasker Clinical Medical Research Award. TNF defined as a therapeutic target for rheumatoid arthritis and other autoimmune diseases. Nat. Med. 9, 1245.

Gilchrist, A., Au, C.E., Hiding, J., Bell, A.W., Fernandez-Rodriguez, J., Lesimple, S., Nagaya, H., Roy, L., Gosline, S.J., Hallett, M., Paiement, J., Kearney, R.E., Nilsson, T., Bergeron, J.J., 2006. Quantitative proteomics analysis of the secretory pathway. Cell 127, 1265.

Gollob, J.A., Veenstra, K.G., Parker, R.A., Mier, J.W., McDermott, D.F., Clancy, D., Tutin, L., Koon, H., Atkins, M.B., 2003. Phase I trial of concurrent twice-weekly recombinant human interleukin-12 plus low-dose IL-2 in patients with melanoma or renal cell carcinoma. J. Clin. Oncol. 21, 2564.

Heller, R.A., Song, K., Fan, N., Chang, D.J., 1992. The p70 tumor necrosis factor receptor mediates cytotoxicity. Cell 70, 47.

Jacobs, M., Togbe, D., Fremond, C., Samarina, A., Allie, N., Botha, T., Carlos, D., Parida, S.K., Grivennikov, S., Nedospasov, S., Monteiro, A., Le Bert, M.,

Quesniaux, V., Ryffel, B., 2007. Tumor necrosis factor is critical to control tuberculosis infection. Microbes Infect. 9, 623.

Katayama, K., Wada, K., Miyoshi, H., Ohashi, K., Tachibana, M., Furuki, R., Mizuguchi, H., Hayakawa, T., Nakajima, A., Kadowaki, T., Tsutsumi, Y., Nakagawa, S., Kamisaki, Y., Mayumi, T., 2004. RNA interfering approach for clarifying the PPARgamma pathway using lentiviral vector expressing short hairpin RNA. FEBS Lett. 560, 178.

Krippner-Heidenreich, A., Tubing, F., Bryde, S., Willi, S., Zimmermann, G., Scheurich, P., 2002. Control of receptor-induced signaling complex formation by the kinetics of ligand/receptor interaction. J. Biol. Chem. 277, 44155.

Margolin, K., Aronson, F.R., Sznol, M., Atkins, M.B., Gucalp, R., Fisher, R.I., Sunderland, M., Doroshow, J.H., Ernest, M.L., Mier, J.W., et al., 1994. Phase II studies of recombinant human interleukin-4 in advanced renal cancer and malignant melanoma. J. Immunother. Emphas. Immunol. 15, 147.

Micheau, O., Tschopp, J., 2003. Induction of TNF receptor I-mediated apoptosis via two sequential signaling complexes. Cell 114, 181.

Miyoshi, H., Smith, K.A., Mosier, D.E., Verma, I.M., Torbett, B.E., 1999. Transduction of human CD34+ cells that mediate long-term engraftment of NOD/SCID mice by HIV vectors. Science 283, 682.

Nathan, D.M., Angus, P.W., Gibson, P.R., 2006. Hepatitis B and C virus infections and anti-tumor necrosis factor-alpha therapy: guidelines for clinical approach. J. Gastroenterol. Hepatol. 21, 1366.

Oh, P., Li, Y., Yu, J., Durr, E., Krasinska, K.M., Carver, L.A., Testa, J.E., Schnitzer, J.E., 2004. Subtractive proteomic mapping of the endothelial surface in lung and solid tumours for tissue-specific therapy. Nature 429, 629.

Schneeweiss, S., Setoguchi, S., Weinblatt, M.E., Katz, J.N., Avorn, J., Sax, P.E., Levin, R., Solomon, D.H., 2007. Anti-tumor necrosis factor alpha therapy and the risk of serious bacterial infections in elderly patients with rheumatoid arthritis. Arthritis Rheum. 56, 1754.

Shibata, H., Yoshioka, Y., Ikemizu, S., Kobayashi, K., Yamamoto, Y., Mukai, Y., Okamoto, T., Taniai, M., Kawamura, M., Abe, Y., Nakagawa, S., Hayakawa, T., Nagata, S., Yamagata, Y., Mayumi, T., Kamada, H., Tsutsumi, Y., 2004. Functionalization of tumor necrosis factor-alpha using phage display technique and PEGylation improves its antitumor therapeutic window. Clin. Cancer Res. 10, 8293.

Shibata, H., Yoshioka, Y., Ohkawa, A., Minowa, K., Mukai, Y., Abe, Y., Taniai, M., Nomura, T., Kayamuro, H., Nabeshi, H., Sugita, T., Imai, S., Nagano, K., Yoshikawa, T., Fujita, T., Nakagawa, S., Yamamoto, A., Ohta, T., Hayakawa, T., Mayumi, T., Vandenabeele, P., Aggarwal, B.B., Nakamura, T., Yamagata, Y., Tsunoda, S., Kamada, H., Tsutsumi, Y., 2008. Creation and X-ray structure analysis of the tumor necrosis factor receptor-1-selective mutant of a tumor necrosis factor-alpha antagonist. J. Biol. Chem. 283, 998.

Stanger, B.Z., Leder, P., Lee, T.H., Kim, E., Seed, B., 1995. RIP: a novel protein containing a death domain that interacts with Fas/APO-1 (CD95) in yeast and causes cell death. Cell 81, 513.

Szlosarek, P.W., Balkwill, F.R., 2003. Tumour necrosis factor alpha: a potential target for the therapy of solid tumours. Lancet Oncol. 4, 565.

Vandenabeele, P., Declercq, W., Beyaert, R., Fiers, W., 1995. Two tumour necrosis factor receptors: structure and function. Trends Cell Biol. 5, 392.

Vandenabeele, P., Declercq, W., Vercammen, D., Van de Craen, M., Grooten, J., Loetscher, H., Brockhaus, M., Lesslauer, W., Fiers, W., 1992. Functional characterization of the human tumor necrosis factor receptor p75 in a transfected rat/mouse T cell hybridoma. J. Exp. Med. 176, 1015.

Wajant, H., Pfizenmaier, K., Scheurich, P., 2003. Tumor necrosis factor signaling. Cell Death Differ. 10, 45.

Weiss, T., Grell, M., Siemienski, K., Muhlenbeck, F., Durkop, H., Pfizenmaier, K., Scheurich, P., Wajant, H., 1998. TNFR80-dependent enhancement of TNFR60-induced cell death is mediated by TNFR-associated factor 2 and is specific for TNFR60. J. Immunol. 161, 3136.

Xu, H., Sethi, J.K., Hotamisligil, G.S., 1999. Transmembrane tumor necrosis factor (TNF)-alpha inhibits adipocyte differentiation by selectively activating TNF receptor 1. J. Biol. Chem. 274, 26287.

Yamamoto, Y., Tsutsumi, Y., Yoshioka, Y., Nishibata, T., Kobayashi, K., Okamoto, T., Mukai, Y., Shimizu, T., Nakagawa, S., Nagata, S., Mayumi, T., 2003. Site-specific PEGylation of a lysine-deficient TNF-alpha with full bioactivity. Nat. Biotechnol. 21, 546.

doi:10.1016/j.jmb.2008.05.047 J. Mol. Biol. (2008) 380, 777–782

JMB

Available online at www.sciencedirect.com

ScienceDirect

ELSEVIER

COMMUNICATION

Organelle-Targeted Delivery of Biological Macromolecules Using the Protein Transduction Domain: Potential Applications for Peptide Aptamer Delivery into the Nucleus

Tomoaki Yoshikawa[1,2]†, Toshiki Sugita[1,2]†, Yohei Mukai[1,2], Natsue Yamanada[1,2], Kazuya Nagano[1,2], Hiromi Nabeshi[1,2], Yasuo Yoshioka[1,3], Shinsaku Nakagawa[2], Yasuhiro Abe[1], Haruhiko Kamada[1,3], Shin-ichi Tsunoda[1,3]* and Yasuo Tsutsumi[1,2,3]

[1]*Laboratory of Pharmaceutical Proteomics, National Institute of Biomedical Innovation, 7-6-8 Saito-Asagi, Ibaraki, Osaka 567-0085, Japan*

[2]*Graduate School of Pharmaceutical Sciences, Osaka University, 1-6 Yamadaoka, Suita, Osaka 565-0871, Japan*

[3]*The Center for Advanced Medical Engineering and Informatics, Osaka University, 1-6 Yamadaoka, Suita, Osaka 565-0871, Japan*

Received 5 March 2008; received in revised form 16 May 2008; accepted 21 May 2008
Available online 29 May 2008

Edited by J. Karn

Extensive effort is currently being expended on the innovative design and engineering of new molecular carrier systems for the organelle-targeted delivery of biological cargoes (e.g., peptide aptamers or biological proteins) as tools in cell biology and for developing novel therapeutic approaches. Although cell-permeable Tat peptides are useful carriers for delivering biological molecules into the cell, much internalized Tat-fused cargo is trapped within macropinosomes and thus not delivered into organelles. Here, we devised a novel intracellular targeting technique to deliver Tat-fused cargo into the nucleus using an endosome-disruptive peptide (hemagglutinin-2 subunit) and a nuclear localization signal peptide. We show for the first time that Tat-conjugated peptide aptamers can be selectively delivered to the nucleus by using combined hemagglutinin-2 subunit and nuclear localization signal peptides. This nuclear targeting technique resulted in marked enhancement of the cytostatic activity of a Tat-fused p53-derived peptide aptamer against human MDM2 (mouse double minute 2) that inhibits p53–MDM2 binding. Thus, our technique provides a unique methodology for the development of novel therapeutic approaches based on intracellular targeting.

Keywords: Tat; HA2; nuclear localization signal; intracellular targeting; peptide aptamer

Progress in molecular biological research on intractable diseases such as cancer is steadily increasing our knowledge of the mechanisms of malignant transformation occurring in tumor cells. However, the complexity of biological interactions makes it increasingly difficult to predict gene and protein functions as we proceed from the immediate metabolic pathway to the levels of the cell and organism. Especially at the cellular level, a variety of tools are available to determine protein function and to develop novel therapeutic approaches, including antisense, peptide modulators, proteins and the overexpression of wild-type or dominant-negative proteins. Small peptides might be able to complement these agents because of

T.S. and T.Y. contributed equally to this work.

*Corresponding author. Laboratory of Pharmaceutical Proteomics, National Institute of Biomedical Innovation, 7-6-8 Saito-Asagi, Ibaraki, Osaka 567-0085, Japan. E-mail address: tsunoda@nibio.go.jp.

† T.S. and T.Y. contributed equally to this work.

Abbreviations used: MDM2, mouse double minute 2; PTD, protein transduction domain; HA2, hemagglutinin-2 subunit; NLS, nuclear localization signal; NLS–VENUS–Tat, VENUS protein with Tat, NLS and His tag; Tat–cargo, Tat-fused cargo; HA2–Tat, Tat-fused endosome-disruptive HA2 peptide; PM10–Tat, Tat-fused PM10; NLS–PM10–

their ability to recognize specific protein domains and thus to interfere with enzymatic functions or protein–protein interactions.[1] Furthermore, these peptides, designated "peptide aptamers," seem to be non-genotoxic and useful for adjunct chemotherapy. However, these approaches are often limited by an inability to effectively deliver the agents to the appropriate cellular location.

Because a prerequisite for their intracellular action is their delivery into cells, various intracellular delivery approaches, such as protein transduction technology with protein transduction domains (PTDs; e.g., Tat, Antp, VP22, Rev and so on), are currently undergoing intensive scrutiny.[2,3] However, protein transduction technology using PTDs has some disadvantages, one of which is the accumulation of PTDs or PTD-fused peptides in the endocytic compartment. We and others have reported that the main mechanism of protein transduction is penetration into cells by macropinocytosis and that therefore much of the material taken up remains entrapped in the macropinosomes.[4–7] Another disadvantage is that there is no technique for controlling the intracellular distribution of peptide aptamers such that their effects are extremely limited. For these reasons, it is important that peptide aptamers be delivered directly into specific cellular compartments. Because optimal approaches for overcoming these disadvantages have not yet been developed, high concentrations of PTDs or PTD-fused peptides must still be employed in order for the technology to function effectively.

With this in mind, we focused on developing intracellular targeting technology for peptide aptamers fused with Tat protein basic domain residues 47–57 (YGRKKRRQRRR) from human immunodeficiency virus-1 in the context of cancer therapeutics. We recently reported that survivin-targeted peptide aptamers (shepherdin) linked to the NH_2-terminal domain of the influenza virus hemagglutinin-2 subunit (HA2), which is a pH-dependent fusogenic peptide inducing lysis of membranes at low pH levels,[8,9] are efficiently released from macropinosomes. This approach succeeded in inducing the death of survivin-expressing malignant tumor cells.[10] Based on this previous study, here we devised a novel intracellular targeting technology using HA2 and nuclear localization signal (NLS) peptides for converting peptide aptamers into efficient research tools for cell biology and cancer therapeutics. We established for the first time that Tat-conjugated peptide aptamers can be selectively delivered to the nucleus by combining HA2 and NLS peptides. Furthermore, we evaluated the utility of our nuclear targeting method using p53-derived peptide from the human MDM2 (mouse double minute 2, also termed HDM2 in humans)-binding domain (residues 17–26: designated PM10), which is a peptide inhibitor of p53–MDM2 binding.[11] Recent reports suggested that inhibiting p53–MDM2 binding could reactivate the p53 pathway and induce growth-suppressive effects and cell cycle arrest of tumor cells as well as normal cells possessing wild-type p53.[11–17] Because the interaction of p53 and MDM2 takes place inside the nucleus, nuclear delivery of PM10 may potentiate the cytostatic effect of this agent. Indeed, we found that our nuclear targeting technique employing PTD, HA2 and NLS peptides markedly enhanced PM10-mediated cytostatic effects against A549 (human lung adenocarcinoma) and WI-38 (human embryonic fibroblast, lung-derived cell line) cells. These results indicate that our intracellular targeting techniques can deliver the cargo into the appropriate organelle and provide a unique research tool for cellular biology and the development of novel therapeutic approaches.

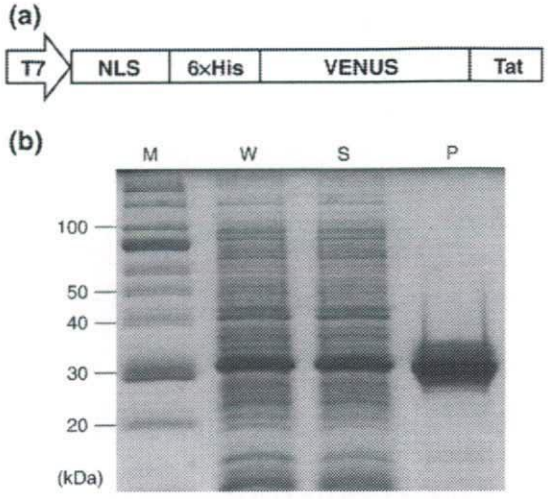

Fig. 1. Vector construction and SDS-PAGE analysis of NLS–VENUS–Tat. (a) Schematic of the NLS–VENUS–Tat region of T7 promoter-driven protein expression vector. The VENUS (variant of yellow fluorescent protein) DNA sequence was kindly provided by Dr. A. Miyawaki (RIKEN Brain Science Institute, Saitama, Japan). The NLS–VENUS–Tat DNA sequence was amplified by PCR. At the 5′ end, the primer sequence 5′-AA CTT TAA GAA GGA GAT ATA *CAT ATG* CCG AAA AAG AAA CGT AAA GTT ACC ATG GCT CAC CAC CAT CAC CAC CAT **GAC TAC AAA GAC GAT GAT GAC AAA** GAA GCT TAC GTG AGC AAG GGC GAG GAG CTG TT-3′ introduced an NdeI site (italics), an NLS (boldface) and a 6× His tag (underline); at the 3′ end, the primer sequence 5′-T TCC TTT CGG GCT TTG TTA GCA GCC *GAA TTC* TTA TTA **ACG GCG ACG CTG GCG ACG TTT TTT ACG ACC GTA** CTC GAG CTT GTA CAG CTC GTC CAT GCC GAG-3′ introduced an EcoRI site (italics) and a Tat sequence (boldface). The PCR product was digested with NdeI as well as EcoRI and inserted into pT7 vector, under the control of the T7 promoter. (b) The plasmid was transformed into *E. coli* BL21 Star (DE3) (Invitrogen, Carlsbad, CA), and cells expressing VENUS proteins were cultured at 25 °C, 250 rpm, for 6 h. The cell paste was then solubilized in a BugBuster Master Mix (Novagen, Darmstadt, Germany) and centrifuged. NLS–VENUS–Tat was recovered in the supernatant and purified by His-tag affinity purification and gel-filtration chromatography. SDS-PAGE analysis was performed under reducing conditions. Lane M, molecular weight standard; lane W, *E. coli* extracts prepared after induction of expression by IPTG; lane S, soluble fractions; lane P, purified proteins.

Tat-fused cargo can be selectively delivered to the nucleus by combining HA2 and NLS peptides

We constructed a VENUS protein (variant of yellow fluorescent protein) fused with Tat, NLS and His tag (NLS–VENUS–Tat) for use as an expression vector (Fig. 1a). NLS–VENUS–Tat was indeed expressed in *Escherichia coli* [BL21 Star (DE3)] after induction with IPTG. The level of expression of the NLS–VENUS–Tat protein was analyzed by SDS-PAGE in total cell lysates (Fig. 1b). Protein expression was specifically induced because we did not find substantially leaky expression of the recombinant protein (data not shown). Recombinant NLS–VENUS–Tat was produced almost entirely in the soluble fraction and had an apparent molecular mass of about 32 kDa under reducing conditions (Fig. 1b, lane S). Purification was carried out by lysis, and separation of the soluble fraction was carried out by centrifugation. This was then loaded onto a Ni^{2+} column for initial purification. The NLS–VENUS–Tat protein eluted from the Ni^{2+} column was more than 90% pure (Fig. 1b, lane P). The purity, apparent molecular mass and cellular internalization activity of the eluted NLS–VENUS–Tat proteins were established by SDS-PAGE and flow cytometry.

Numerous mechanistic studies have shown that Tat peptides rapidly permeate plasma membranes and translocate into the nucleus.[18–22] This mechanism is currently used to deliver proteins and nucleic acids to cell nuclei through covalent linkages of Tat and cargoes.[18] However, nuclear delivery has remained problematic and very limited, because endosome escape and nuclear transport of Tat-fused cargo (Tat–cargo) represent a passive rather than an active process. Indeed, in HeLa cells treated with NLS–VENUS–Tat alone, only punctate cytoplasmic fluorescence, and no fluorescence in the nucleus, was observed (Fig. 2). We had previously confirmed that Tat-fused VENUS co-localized in live cells to vesicles with FM4-64, which is a general endosome marker (data not shown). Furthermore, FAM (carboxyfluorescein) dye-fused Tat peptides also co-localized in FM4-64-positive endosomal vesicles (data not shown). Thus, these results indicated that much of the NLS–VENUS–Tat was entrapped within the endosomal vesicles, resulting in low levels of nuclear accumulation. It is therefore reasonable to propose that Tat–cargo alone cannot reach the targeted cellular compartment, especially the nucleus, and that the therapeutic effects of anticancer peptide aptamers are extremely limited for this reason. Therefore, we devised an active nuclear targeting technique using endosome-disruptive HA2 and SV40-derived NLS peptides.

Recently, we reported that co-treatment with Tat–cargo and the Tat-fused endosome-disruptive HA2 peptide (HA2–Tat) improved the endosome-escape ability and the tumor-killing activity of Tat-fused antisurvivin peptide aptamers.[10] Therefore, we hypothesized that NLS–VENUS–Tat can be delivered into the nucleus if NLS–VENUS–Tat can be engineered to escape from the endosomal vesicles into the cytosol by co-treatment with HA2–Tat. To investigate whether co-treatment with HA2–Tat does effectively improve the nuclear localization of NLS–Tat–cargo, we co-treated HeLa cells with NLS–VENUS–Tat and HA2–Tat and analyzed the intracellular localization of NLS–VENUS–Tat by confocal laser scanning

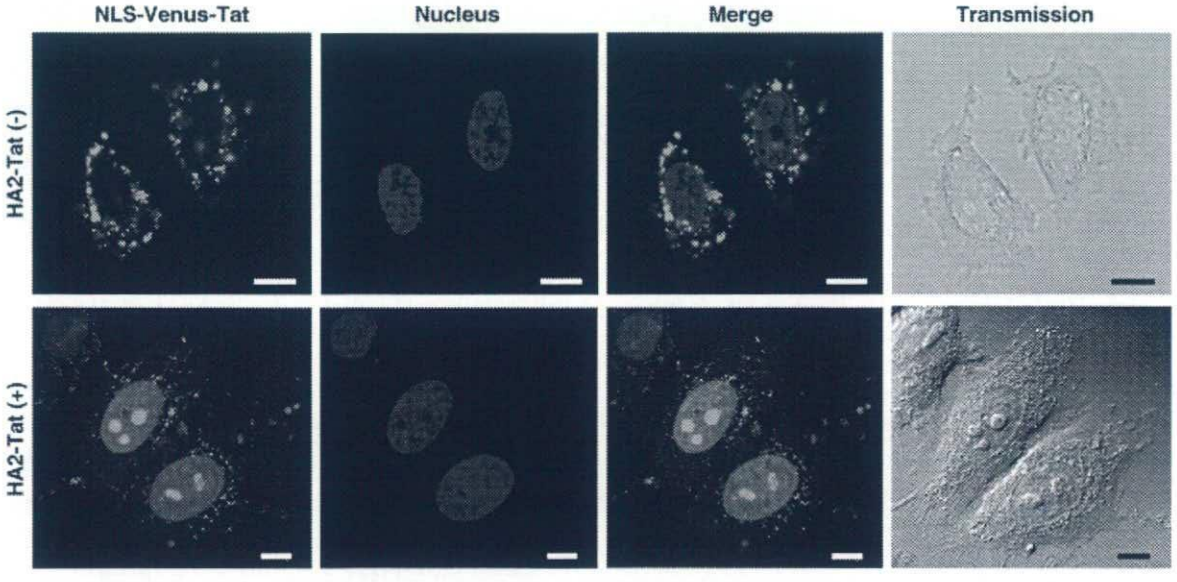

Fig. 2. Intracellular distribution of NLS–VENUS–Tat. HeLa cells were cultured on a Lab-Tek II Chambered Coverglass system (Nalge Nunc International) at 3.0×10^4 cells/well in MEM (minimum essential medium)-α supplemented with 10% fetal bovine serum and incubated for 24 h at 37 °C. Internalization of NLS–VENUS–Tat was performed as follows: HeLa cells were co-treated with NLS–VENUS–Tat (10 μM) with or without HA2–Tat (5 μM) in Opti-MEM I (Invitrogen) containing 100 ng/ml of Hoechst 33342 (Invitrogen). After incubation at 37 °C for 3 h, the medium was changed for a fresh medium and assessed by confocal laser scanning microscopy (Leica Microsystems GmbH, Wetzlar, Germany) without cell fixation. Scale bars in each photomicrograph represent 10 μm.

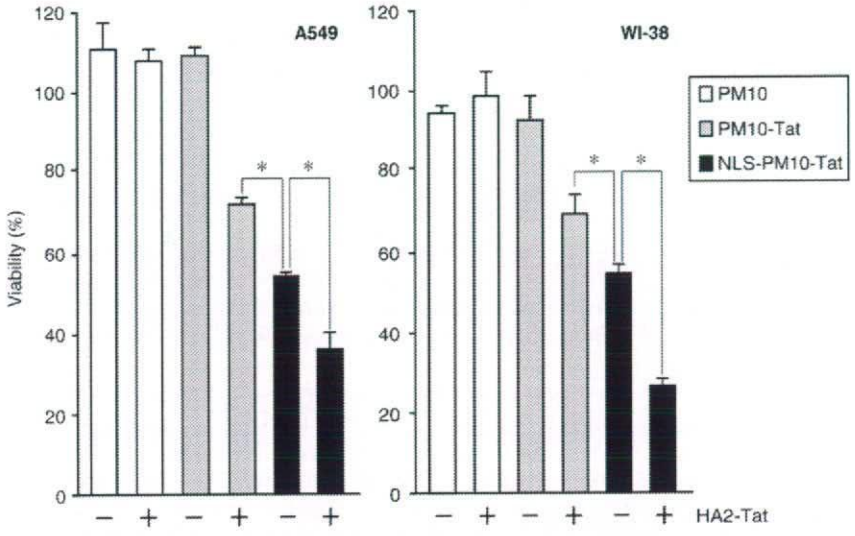

Fig. 3. Nuclear targeting potentiates the cytostatic effect of PM10. All peptides used in this study were purchased from GL Biochem Ltd. (Hiroshima, Japan) with confirmed purities >90% by HPLC and mass spectrography. The sequences of these peptides were GLFEAIEGFIENGWEGMIDGWYG**YGRKKRRQRRR** for HA2–Tat, ETFSDLWKLL for PM10, ETFSDLWKLL**YGRKKRRQRRR** for PM10–Tat and PKKKRKVETFSDLWKLL**YGRKKRRQRRR** for NLS–PM10–Tat. Tat and NLS are shown in boldface and underlined, respectively. A549 or WI-38 cells were seeded into 96-well tissue culture plates (Nalge Nunc International) at 1.0×10^4 cells/well. After incubation for 24 h at 37 °C, the cells were treated with PM10, PM10–Tat or NLS–PM10–Tat at 6 μM (for A549 cells) or 12 μM (for WI-38 cells) in the presence or absence of HA2–Tat (5 μM). After 6 h (for A549 cells) or 24 h (for WI-38 cells), cell viability was determined with the use of WST-8 assay (Nakalai Tesque Inc., Kyoto, Japan) according to the manufacturer's protocol. Data are presented as the mean±SD of triplicate assays. Statistical treatment of the data was performed according to Student's *t* test for two populations (*$p<0.01$).

microscopy (Fig. 2). Co-treatment of HeLa cells with NLS–VENUS–Tat and HA2–Tat resulted in nuclear localization of VENUS, co-localized with Hoechst 33342-stained nuclei. This finding documents that Tat–cargo can be selectively delivered to the nucleus by using HA2 and NLS peptides. Although several groups have attempted to deliver macromolecular drugs to specific organelles, they used PTDs conjugated only with an organelle-targeting signal, such as NLS or mitochondria-targeting signal.[23,24,25] Our data revealed that NLS–VENUS–Tat was entrapped within the endosomal vesicles, with no detectable fluorescence derived from VENUS found in the nucleus. This indicates that organelle targeting by signal-fused PTD–cargo alone does not allow efficient migration into the targeted organelle in the absence of an endosome-escape strategy. Although the influence of the use of different cell types, fluorescent dye, cargo, incubation time and so on could not be excluded as contributing to targeting inability, we found that nuclear transport efficiency could be augmented by combining PTD, HA2 and NLS peptides. Furthermore, our results imply that macromolecules could be delivered into other organelles, such as mitochondria, endoplasmic reticulum and peroxisomes, using different organelle-targeting signal sequences. To this end, we are currently developing novel intracellular drug delivery systems that can target macromolecules into different organelles in a manner analogous to our nuclear targeting techniques.

Nuclear targeting enhances the cytostatic activity of anti-MDM2 peptide aptamer

Next, we tested the utility of our nuclear targeting method using the MDM2-binding peptide aptamer, PM10, which is a p53-derived peptide corresponding to a sequence within the MDM2-binding domain. Kanovsky *et al.* reported that PTD-mediated intracellular delivery of PM10 could reactivate p53 and induce p53-mediated apoptosis of tumor cells with wild-type p53.[11] Under physiological conditions, growth-suppressive and proapoptotic activity of p53 is inhibited by MDM2, which binds p53 and negatively regulates its activity and stability.[16] Recent reports indicated that prevention of p53–MDM2 binding activates the p53 signaling pathway and induces p53-dependent apoptosis in cancer cells possessing wild-type p53.[12,14,15] In addition, the abrogation of p53–MDM2 binding mediates a cytostatic effect and cell cycle arrest in proliferating normal cells.[13,15,17] Because PM10 seems to bind nuclear-localized MDM2 and inhibits MDM2-inducible ubiquitination and degradation of p53, we hypothesized that the nuclear targeting method using HA2 and NLS peptides would enhance its cytotoxicity. To test this, we investigated the effects of treatment with PM10 on cell viability using A549 (human lung adenocarcinoma) and WI-38 (human lung-derived embryonic fibroblast) cells, which possess wild-type p53 (Fig. 3). In A549 and WI-38 cells treated with PM10, Tat-fused PM10 (PM10–Tat) grew vigorously. However, co-treatment with HA2–Tat and PM10–Tat together markedly inhibited A549 and WI-38 cell growth. Furthermore, A549 and WI-38 cells co-treated with HA2–Tat and NLS-fused PM10–Tat (NLS–PM10–Tat) showed greater growth inhibition compared with those treated with NLS–PM10–Tat alone. According to a report from the developers of PM10, although transduction of PTD-fused PM10 (PM10-PTD) into cancer cells could induce tumor cell death *in vitro* and *in vivo*, a high concentration of PM10-PTD was required to see an effect on cancer

cells.[11,26] In contrast, our nuclear targeting technique using PTD, HA2 and NLS peptides markedly enhanced the nuclear localization of the cargo and the PM10-mediated cytostatic effect at low concentrations of PM10. To the best of our knowledge, this is the first report that nuclear targeting of MDM2-binding peptide aptamers can lead to augmentation of cytostatic activity.

In the present study, we aimed to develop a novel cancer therapeutic approach by controlling apoptotic pathways using peptide-based drugs. Recently, the use of intracellular antibodies (intrabodies) directed to a specific target antigen present in the cell has also been suggested as a therapeutic lead to control the apoptotic pathway.[27,28] Our organelle-targeting strategy does seem able to deliver intrabodies directly to the specific organelle in which disease-related proteins reside. Furthermore, we have generated antibodies for various targeted antigens using a non-immune phage scFv library.[29] Thus, we are also currently developing a novel approach to intracellular therapy combining an organelle-targeting strategy and antibody engineering.

Acknowledgements

This study was supported in part by Grants-in-Aid for Scientific Research (20790156) from the Ministry of Education, Culture, Sports, Science and Technology of Japan; in part by a Health and Labor Sciences Research Grant from the Ministry of Health, Labor and Welfare of Japan; in part by a Grant for Industrial Technology Research Program (03A47016a) from the New Energy and Industrial Technology Development Organization of Japan; and in part by funding from the Takeda Science Foundation.

References

1. Mendoza, F. J., Espino, P. S., Cann, K. L., Bristow, N., McCrea, K. & Los, M. (2005). Anti-tumor chemotherapy utilizing peptide-based approaches—apoptotic pathways, kinases, and proteasome as targets. *Arch. Immunol. Ther. Exp.* **53**, 47–60.
2. Dietz, G. P. & Bahr, M. (2004). Delivery of bioactive molecules into the cell: the Trojan horse approach. *Mol. Cell. Neurosci.* **27**, 85–131.
3. Chauhan, A., Tikoo, A., Kapur, A. K. & Singh, M. (2007). The taming of the cell penetrating domain of the HIV Tat: myths and realities. *J. Controlled Release*, **117**, 148–162.
4. Fretz, M., Jin, J., Conibere, R., Penning, N. A., Al-Taei, S., Storm, G. *et al.* (2006). Effects of Na^+/H^+ exchanger inhibitors on subcellular localisation of endocytic organelles and intracellular dynamics of protein transduction domains HIV-TAT peptide and octaarginine. *J. Controlled Release*, **116**, 247–254.
5. Wadia, J. S., Stan, R. V. & Dowdy, S. F. (2004). Transducible TAT-HA fusogenic peptide enhances escape of TAT-fusion proteins after lipid raft macropinocytosis. *Nat. Med.* **10**, 310–315.
6. Sugita, T., Yoshikawa, T., Mukai, Y., Yamanada, N., Imai, S., Nagano, K. *et al.* (2008). Comparative study on transduction and toxicity of protein transduction domains. *Br. J. Pharmacol.* **153**, 1143–1152.
7. Kaplan, I. M., Wadia, J. S. & Dowdy, S. F. (2005). Cationic TAT peptide transduction domain enters cells by macropinocytosis. *J. Controlled Release*, **102**, 247–253.
8. Han, X., Bushweller, J. H., Cafiso, D. S. & Tamm, L. K. (2001). Membrane structure and fusion-triggering conformational change of the fusion domain from influenza hemagglutinin. *Nat. Struct. Biol.* **8**, 715–720.
9. Skehel, J. J., Cross, K., Steinhauer, D. & Wiley, D. C. (2001). Influenza fusion peptides. *Biochem. Soc. Trans.* **29**, 623–626.
10. Sugita, T., Yoshikawa, T., Mukai, Y., Yamanada, N., Imai, S., Nagano, K. *et al.* (2007). Improved cytosolic translocation and tumor-killing activity of Tat-shepherdin conjugates mediated by co-treatment with Tat-fused endosome-disruptive HA2 peptide. *Biochem. Biophys. Res. Commun.* **363**, 1027–1032.
11. Kanovsky, M., Raffo, A., Drew, L., Rosal, R., Do, T., Friedman, F. K. *et al.* (2001). Peptides from the amino terminal mdm-2-binding domain of p53, designed from conformational analysis, are selectively cytotoxic to transformed cells. *Proc. Natl. Acad. Sci. USA*, **98**, 12438–12443.
12. Vassilev, L. T., Vu, B. T., Graves, B., Carvajal, D., Podlaski, F., Filipovic, Z. *et al.* (2004). *In vivo* activation of the p53 pathway by small-molecule antagonists of MDM2. *Science*, **303**, 844–848.
13. Vassilev, L. T. (2004). Small-molecule antagonists of p53–MDM2 binding: research tools and potential therapeutics. *Cell Cycle*, **3**, 419–421.
14. Tovar, C., Rosinski, J., Filipovic, Z., Higgins, B., Kolinsky, K., Hilton, H. *et al.* (2006). Small-molecule MDM2 antagonists reveal aberrant p53 signaling in cancer: implications for therapy. *Proc. Natl. Acad. Sci. USA*, **103**, 1888–1893.
15. Shangary, S., Qin, D., McEachern, D., Liu, M., Miller, R. S., Qiu, S. *et al.* (2008). Temporal activation of p53 by a specific MDM2 inhibitor is selectively toxic to tumors and leads to complete tumor growth inhibition. *Proc. Natl. Acad. Sci. USA*, **105**, 3933–3938.
16. Kubbutat, M. H., Jones, S. N. & Vousden, K. H. (1997). Regulation of p53 stability by Mdm2. *Nature*, **387**, 299–303.
17. Efeyan, A., Ortega-Molina, A., Velasco-Miguel, S., Herranz, D., Vassilev, L. T. & Serrano, M. (2007). Induction of p53-dependent senescence by the MDM2 antagonist nutlin-3a in mouse cells of fibroblast origin. *Cancer Res.* **67**, 7350–7357.
18. Vives, E., Charneau, P., van Rietschoten, J., Rochat, H. & Bahraoui, E. (1994). Effects of the Tat basic domain on human immunodeficiency virus type 1 transactivation, using chemically synthesized Tat protein and Tat peptides. *J. Virol.* **68**, 3343–3353.
19. Vives, E., Brodin, P. & Lebleu, B. (1997). A truncated HIV-1 Tat protein basic domain rapidly translocates through the plasma membrane and accumulates in the cell nucleus. *J. Biol. Chem.* **272**, 16010–16017.
20. Potocky, T. B., Menon, A. K. & Gellman, S. H. (2003). Cytoplasmic and nuclear delivery of a TAT-derived peptide and a beta-peptide after endocytic uptake into HeLa cells. *J. Biol. Chem.* **278**, 50188–50194.
21. Caron, N. J., Quenneville, S. P. & Tremblay, J. P. (2004). Endosome disruption enhances the functional nuclear delivery of Tat-fusion proteins. *Biochem. Biophys. Res. Commun.* **319**, 12–20.

22. Lundberg, M., Wikstrom, S. & Johansson, M. (2003). Cell surface adherence and endocytosis of protein transduction domains. *Mol. Ther.* **8**, 143–150.
23. Shokolenko, I. N., Alexeyev, M. F., LeDoux, S. P. & Wilson, G. L. (2005). TAT-mediated protein transduction and targeted delivery of fusion proteins into mitochondria of breast cancer cells. *DNA Repair (Amst.)*, **4**, 511–518.
24. Del Gaizo, V. & Payne, R. M. (2003). A novel TAT-mitochondrial signal sequence fusion protein is processed, stays in mitochondria, and crosses the placenta. *Mol. Ther.* **7**, 720–730.
25. Matsushita, M., Tomizawa, K., Moriwaki, A., Li, S. T., Terada, H. & Matsui, H. (2001). A high-efficiency protein transduction system demonstrating the role of PKA in long-lasting long-term potentiation. *J. Neurosci.* **21**, 6000–6007.
26. Michl, J., Scharf, B., Schmidt, A., Huynh, C., Hannan, R., von Gizycki, H. *et al.* (2006). PNC-28, a p53-derived peptide that is cytotoxic to cancer cells, blocks pancreatic cancer cell growth *in vivo*. *Int. J. Cancer*, **119**, 1577–1585.
27. Wheeler, Y. Y., Kute, T. E., Willingham, M. C., Chen, S. Y. & Sane, D. C. (2003). Intrabody-based strategies for inhibition of vascular endothelial growth factor receptor-2: effects on apoptosis, cell growth, and angiogenesis. *FASEB J.* **17**, 1733–1735.
28. Williams, B. R. & Zhu, Z. (2006). Intrabody-based approaches to cancer therapy: status and prospects. *Curr. Med. Chem.* **13**, 1473–1480.
29. Imai, S., Mukai, Y., Nagano, K., Shibata, H., Sugita, T., Abe, Y. *et al.* (2006). Quality enhancement of the non-immune phage scFv library to isolate effective antibodies. *Biol. Pharm. Bull.* **29**, 1325–1330.

Laboratory of Pharmaceutical Proteomics[1], National Institute of Biomedical Innovation (NIBIO), Graduate School of Pharmaceutical Sciences[2], Center of Advanced Medical Engineering and Informatics[3], Osaka University, Osaka, Japan

Effect of protein properties on display efficiency using the M13 phage display system

S. Imai[1, 2], Y. Mukai[1, 2], T. Takeda[1], Y. Abe[1], K. Nagano[1, 2], H. Kamada[1, 3], S. Nakagawa[2], S. Tsunoda[1, 3], Y. Tsutsumi[1, 2, 3]

Received May 15, 2008, accepted May 21, 2008

Shin-ichi Tsunoda, Ph.D., Laboratory of Pharmaceutical Proteomics, National Institute of Biomedical Innovation (NIBIO), 7-6-8 Saito-Asagi, Ibaraki, Osaka 567-0085, Japan
tsunoda@nibio.go.jp

Pharmazie 63: 760–764 (2008) *doi: 10.1691/ph.2008.8132*

The M13 phage display system is a powerful technology for engineering proteins such as functional mutant proteins and peptides. In this system, it is necessary that the protein is displayed on the phage surface. Therefore, its application is often limited when a protein is poorly displayed. In this study, we attempted to understand the relationship between a protein's properties and its display efficiency using the well-known pIII and pVIII type phage display system. The display of positively charged SV40 NLS and HIV-1 Tat peptides on pIII was less efficient than that of the neutrally charged RGDS peptide. When different molecular weight proteins (1.5–58 kDa) were displayed on pIII and pVIII, their display efficiencies were directly influenced by their molecular weights. These results indicate the usefulness in predicting a desired protein's compatibility with protein and peptide engineering using the phage display system.

1. Introduction

Phage display systems have attracted much attention as the best technology to create functional mutant proteins and peptides ever since Smith et al. reported that random peptides could be displayed on the surface of filamentous M13 phage (Smith 1985). Many researchers have applied this system in attempts to create human antibodies and tissue-specific peptides (Schier et al. 1996; Maruta et al. 2003; Imai et al. 2006). Indeed, we have been successful in creating a useful mutant TNF to be used as a drug (Shibata et al. 2004; Yamamoto et al. 2003). Thus, the phage display system has a wide range of applications (Stich et al. 2003; Gourdine et al. 2005; Takashima et al. 2000).

Filamentous M13 phage has a circular single stranded DNA and takes the form of a long tube that consists of eleven kinds of proteins. This virus effectively proliferates upon infection of *E. coli* (Sidhu 2001; Bayer and Feigenson 1985; Kuhn 1987). In the phage display system, a fusion protein composed of target-molecule and coat protein is derived from a phagemid vector, and wild-type phage composition proteins (pI–pXI) are derived from a helper phage genome. These components can make phage libraries that display target-molecules by assembling within the periplasm of *E. coli*. The most useful characteristic of this system is that protein libraries can be displayed easily on the phage surface by inserting gene libraries within the phage genome. Target-molecules are obtained rapidly by the use of an *in vitro* affinity panning procedure that selects and amplifies specific phage clones (Smith 1985).

In the phage display system, target-molecules can be displayed on coat proteins (pIII, pVI, pVII, pVIII, pIX), though generally they are displayed on pIII or pVIII. Displaying 0–1 molecule per phage in the pIII type phage display system is suitable for isolating high-affinity molecules (Chasteen et al. 2006; Keresztessy et al. 2006). Alternatively, ten molecules can be displayed on a phage particle in the pVIII type phage display system to select low-affinity molecules (Verhaert et al. 1999; Kneissel et al. 1999; Lowman 1997).

As described, the phage display system is the most useful tool to create bioactive peptides and functional mutant proteins. However, because the efficiency of display is influenced by the properties of the target protein (molecular weight, electric charge, etc.), poor display often limits its application. Despite this problem, there is little research examining the relationship between display efficiency and a protein's properties. Thus, studies are warranted in order to apply the phage display system effectively. In this report, we prepared phages that displayed proteins of different molecular weights and electric charges to ascertain the relationship between display efficiency and protein properties.

2. Investigations, results and discussion

In this study we examined the relationship between protein properties (molecular weight, electric charge etc.) and the efficiency of display with pIII and pVIII coat proteins of the filamentous M13 phage display system (Fig. 1). To begin with, we prepared phages that displayed different electrically charged peptides on pIII (Fig. 2B) and evalu-

A)

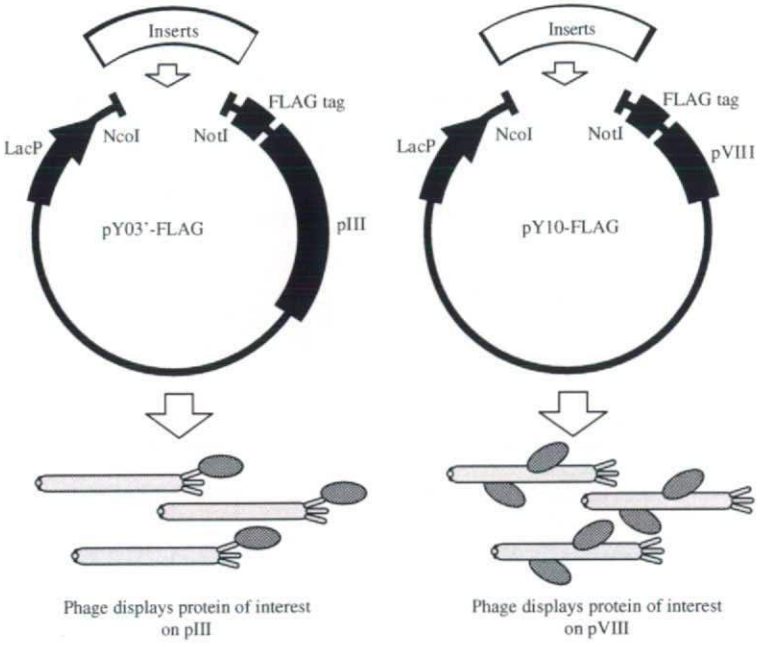

B)

Inserts	Molecular weight (Da)	pI
RGDS peptide (RGDS)	443	6.4
SV40 NLS peptide (PKKKRKV)	883	11.9
HIV-Tat peptide (YGRKKRRQRRR)	1,559	12.8
LacZ-α	11,000	5.2
anti-KDR scFv	25,000	5.0
Importin-α	58,000	5.1

Fig. 1:
Construction of phagemid vectors encoding different proteins or peptides.
A) Different inserts were cloned into pY03′-FLAG and pY10-FLAG phagemid vectors. Phage particles displaying proteins fused to pIII and pVIII were prepared from pY03′-FLAG and pY10-FLAG, respectively. B) Different inserts and their molecular weights

A)

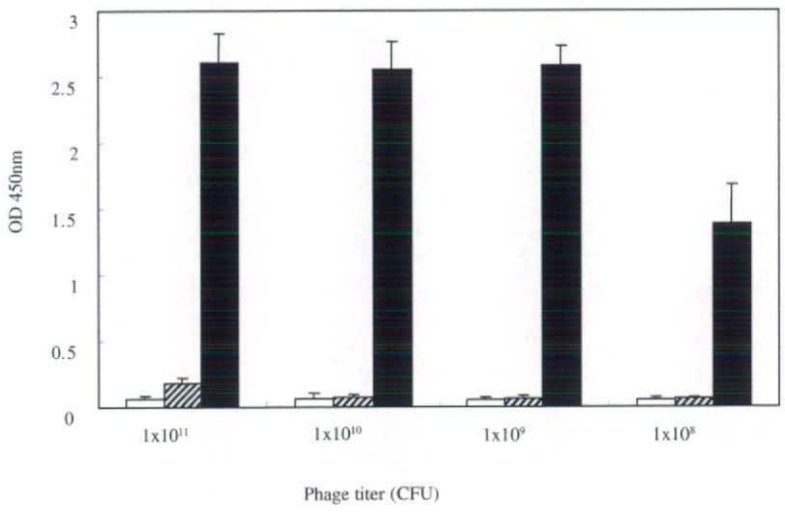

B)

	sequence	M.W. (Da)	pI
□ Tat peptide	YGRKKRRQRRR	1,559	12.8
▩ SV40 NLS	PKKKRKV	883	11.9
■ RGDS peptide	RGDS	433	6.4

Fig. 2:
Influence of the efficiency of peptide-display by the ionic charge of peptides.
The efficiency of peptide-display on pIII was assessed by phage ELISA. Displayed peptides were fused to FLAG-tag – pIII on the phage particle and captured by immobilized anti-FLAG antibody. After washing, the number of captured phage was assessed by anti-M13 HRP conjugate. Two positively charged peptides (Tat peptide; □ and SV40 NLS; ▩) and a neutral peptide (RGDS; ■) were used in this experiment (n = 3). Each data value represents the mean ± S.D. B) Sequences of displayed peptides and their pIs. Cationic amino acids are underlined. All pI values were calculated by Expasy Compute pI/Mw tool (http://au.expasy.org)